Evaluation of the effect of metabolism and transporters on drug pharmacokinetics and
pharmacodynamics using PBPK modeling

by

Lucy Ibrahim Alfred Darakjian

A dissertation submitted to the Graduate Faculty of
Auburn University
in partial fulfillment of the
requirements for the Degree of
Doctor of Philosophy

Auburn, Alabama
May 02, 2020

Keywords: Physiological-based pharmacokinetics; Caffeine; Granisetron; Metabolism; Modeling
and Simulation

Approved by

Amal Kaddoumi, Chair, Professor of Biopharmaceutics
Randall Clark, Professor of Medicinal Chemistry
Jayachandra Ramapuram, Professor of Pharmaceutics
Murali Dhanasekaran, Professor of Pharmacology
Feng Li, Assistant Professor of Pharmaceutics

Abstract

In the latest years, multiple types of computational models have been used extensively in drug development, with a massive growth of uses of physiologically-based pharmacokinetic (PBPK) modeling in fields associated with drugs and natural chemicals. PBPK models are used for systemic and tissue exposure. Combined with the pharmacodynamic models (PD), PBPK models can predict drug-effect over time in many disease states and populations. To attain a mechanistic description of the effect of a drug in biological systems, PBPK models correlated drug-specific data with the biology and physiology at the organism level, permitting a deductive simulation of drug concentration–time profiles. In this dissertation, we studied the effect of transporters and metabolism on the pharmacokinetics (PK) and PD of 2 drugs: caffeine (specifically in pregnant populations), and granisetron using PBPK modeling.

About 80% of pregnant women consume caffeine orally on a daily basis. Many reports indicated that consumption of >200 mg caffeine during pregnancy could increase the likelihood of miscarriage. Thus, we developed and validated a pregnancy PBPK/PD model for caffeine to examine the association between maternal caffeine consumption during pregnancy, and caffeine plasma levels at doses between 70 mg and 300 mg. The developed model was used to predict changes in caffeine concentrations across the 3 trimesters, and to predict associated changes in caffeine PD parameters. The model successfully predicted the effect of decreased cytochrome P450 (CYP1A2) activity on caffeine plasma levels and predicted the increased levels of caffeine in the fetoplacental compartment (FPC). Increased caffeine levels in maternal blood were accompanied by greater inhibition of phosphodiesterase enzyme, higher cyclic adenosine monophosphate, and a greater increase of epinephrine levels, which could increase the risk of pregnancy loss. The application of the developed PBPK model to predict PD effect could provide a useful tool to help define potential cut-offs for caffeine intake in various stages of

pregnancy. Our future directions for this project are to use this project to correlate the amount of caffeine intake during pregnancy to the percent of miscarriage on pregnant subject.

Chemotherapy-induced nausea and vomiting (CINV) is one of the most devastating side effects that affect a patient's quality of life. Granisetron is effective in many cases; however, about 20-30% of patients remain to show unsatisfactory responses, which could be due to the development of drug resistance caused by anti-cancer drugs. The purpose of this project is to explain the observed variability in granisetron efficacy. We started by identifying the effect of P-glycoprotein (P-gp) and lysosomal entrapment on granisetron permeability and plasma profiles following oral dosing. Our predicted results, assessed by in vitro experiments, demonstrated that changes in P-gp function, as well as lysosomal pH, alters granisetron permeability and plasma concentrations. Granisetron is cleared mainly by hepatic metabolism, with less than 20% excreted unchanged in the urine. Granisetron is metabolized primarily by CYP 1A1 and CYP 3A5. Thus, in the second part of the study, we developed a PKPD model to validate and predict the effect of genetic variations in CYP1A1 and CYP3A5 on granisetron levels in plasma and brain and predict the effect of these genetic variations on the occupancy of 5-hydroxytryptamine (5-HT3) receptors. Our results showed that granisetron is a P-gp substrate and is usually effluxed out of the cells, thus limiting its absorption. Also, due to its physicochemical properties, granisetron gets entrapped inside the lysosomes, limiting its passage through cell lines. Furthermore, genetic polymorphism plays an important role in receptor occupancy, where we concluded that subjects with CYP1A1 single nucleotide polymorphism (SNP) (and extensive metabolizer) would lower plasma and brain levels thus decreasing receptor occupancy, while subjects with the CYP3A5 SNP (a poor metabolizer), would have an increase in granisetron levels, thus increasing receptor occupancy for better CINV control.

In conclusion, PBPK models can be invaluable support in drug development. Predicting potential drug effects in several populations is some of the major topics where PBPK approaches have presented significant advances in recent years. Our future directions will be to use PBPK modeling to build models and predict drug effect and doses in several other important populations like the pediatric population, where drug dosing is problematic. Another important direction is the utilization of PBPK modeling in simulating several drug-drug interactions (DDI), especially in geriatric population where most of the patients are on polypharmacy and the possibility of DDI is high.

Table of Contents

List of Tables

List of Figures

List of Schemes

List of Abbreviations

ADME   Absorption, Distribution, Metabolism, Elimination

AP   Area Postremia

AUC   Area Under the Curve

BCS   Biopharmaceutical Classification System

CL   Drug Clearance

CL_{int} Intrinsic Clearance

C_{max} Plasma Maximum Concentration

CNS   Central Nervous System

CTZ   Chemotherapy Trigger Zone

CYP enzymes   Cytochrome P450 enzymes

DDI   Drug- Drug Interaction

DMPK   Drug Metabolism and Pharmacokinetics

EMA   European Medicines Agency

FDA   Food & Drug Administration

fm   Fraction Metabolized

fup   Plasma Fraction Unbound

GFR   Glomerular Filtration Rate

Kp   Partition coefficient

IO   Intraocular administration

IV   Intravenous administration

MDM   Mechanistic Dynamic Model

MSM   Mechanistic Static Model

PBPK   Physiologically Based Pharmacokinetics

PD   Pharmacodynamics

P_{eff} Effective Permeability

PK   Pharmacokinetics

PNS   Peripheral Nervous System

PO   Oral administration

Q   Flow Rate

SC   Subcutaneous administration

T_{max} Time to Reach Maximum Concentration

$T_{1/2}$ Half-life

VD   Volume of Distribution

5-HT3   5-Hydroxytryptamine 3

Chapter 1

Introduction

Brief Introduction about PBPK Models

Physiologically based pharmacokinetics (PBPK) was first introduced in 1937 by Teorell (Paalzow, 2010), the father of pharmacokinetics (PK), where he presented his objective that is to derive "general mathematical relations from which it is possible, in any case for practical purposes, to describe the kinetics of distribution of substances in the body" (Paalzow, 2010). Increasing access to literature data has made it easier to build and refine PBPK models. To predict drug exposure, dose-response, and time-course of pharmacokinetic profiles, kinetic models have been used for different dosage schedules and in several species, disease state, and population. Based on the model's preclinical Absorption, Distribution, Metabolism and excretion (ADME) data, the pharmacokinetic profile of a compound can be predicted, and it can be used to assess drug exposure in a desired organ, taking into account the metabolism within that organ, if applicable. To achieve a desired effect of a certain drug dosage, one should predict the pharmacokinetics (PK) as well as the resultant pharmacodynamic (PD) of that drug. When the PK of a compound is predicted, in combination with the PD model, the effect-time profiles can be estimated, and together with the dosage of the drug can be used to achieve the desired exposure *in-vivo* (Jones, 2013).

Different PK profiles can be predicted in diverse populations of several age and disease states based on PK data from one population. A series of mechanistic equations are used to build PBPK models that usually have certain specifications and restrictions to include different physiological and biological variables through which ADME of many drugs can be defined (Rodgers and Rowland, 2007). Due to the need for several input parameters and the

mathematical difficulty of PBPK models, there is a limitation in the application of PBPK in the pharmaceutical industry (Center for Drug Evaluation and Research (CDER), 2018). As a consequence to that there is a growing availability of several softwares, for instance, GastroPlus (SimulationsPlus, Lancaster, CA) (http://www.simulations-plus.com/), Simcyp Population-Based Simulator (Sheffield, UK) (http://www.simcyp.com/), and PKSIM (Bayer Technology Services, Germany) (http://www.systems-biology.com/products/pk-sim.html) and many others, pharmaceutical companies have shown interest in PBPK modeling applications (Huang *et al.*, 2013).

Regulatory agencies have been requesting pharmaceutical companies to include PBPK model methods when submitting pharmaceutical records (Center for Drug Evaluation and Research (CDER), 2018). The Food and Drug Administration (FDA) has received 33 cases involving PBPK in the years between 2008 and 2012 (FDA, 2017). Lately, both the FDA and the European Medicines Agency (EMA) updated guidance documents on the evaluation of drug–drug interaction (DDI) possibility where the use of PBPK modeling was encouraged by both agencies (FDA, 2017; EMA, 2018).

PBPK Model Methodology and Components

PBPK models are scientific models that incorporate drug-specific information and information on target physiology, to predict drug levels and effect (PK and PD) in both plasma and different tissues (Jones, 2013). PBPK models represent different compartments corresponding body organs, every organ with its blood supply, blood flow, organ volume (or weight), and organ intrinsic clearance (CL_{int}); each of these parameters is specific for a species of interest. Classically, these compartments include the major organs of the body, specifically, adipose, bone, brain, gut, heart, kidney, liver, lung, muscle, skin, and spleen (Rodgers and

Rowland, 2007). Each tissue is expressed with assumptions of either perfusion-rate-limited or permeability-rate-limited. When drug permeability is high, the extent of drug partitioning into the tissue is limited by the blood flow through the tissue (i.e., perfusion limited). Perfusion-rate-limited kinetics assumes a well-stirred model with clearance taking place only by the liver and/or kidneys. Lipophilic compounds tend to follow the perfusion-rate-limited kinetics where the limiting rate for absorption is the tissue blood flow. The partition coefficient (Kp) is used to calculate how much drug is in the tissue, where immediate partitioning is assumed (Holt *et al.*, 2019).
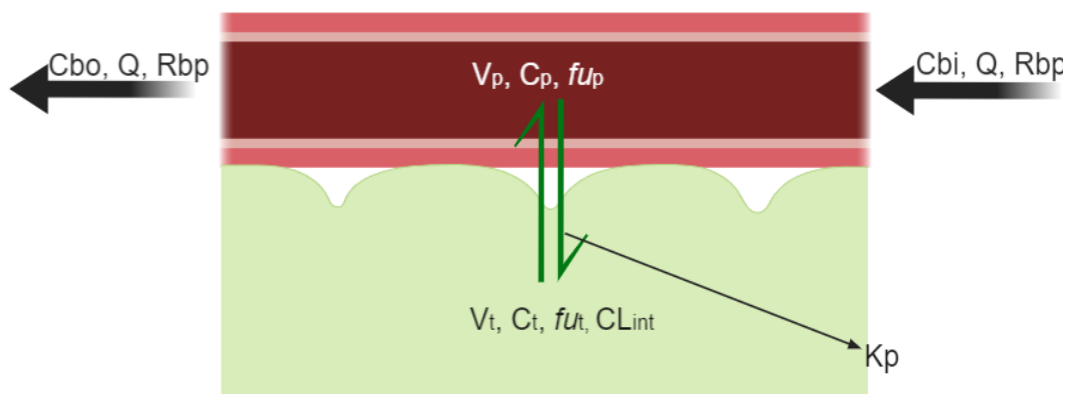
Scheme 1. Schematic view of Perfusion–limited tissues.

Where:

C_{bi}, C_{bo}: Blood concentration entering/leaving the tissue.

R_{bp}: Blood/plasma drug concentration ratios.

V_p, V_t: Plasma and tissue volumes (weight).

C_p, C_t: Plasma and tissue drug concentrations.

K_p: Tissue-plasma partition coefficient.

F_{up}, f_{ut}: Fractions unbound is plasma and tissues.

CL_{int}: tissue intrinsic clearance (if applicable).

Perfusion-limited tissue has no role in drug clearance. The change in drug concentration in the tissue is equivalent to the product of blood flow and the difference between the blood concentrations entering tissue and the ratio of tissue concentration corrected for red blood cell binding divided by Kp as shown in equation 1 (Holt *et al.*, 2019).

$$Vt\frac{dCt}{dt} = Q(Cbi - \frac{Ct \; x \; Rbp}{Kp}) \qquad\qquad\qquad Equation \; 1.$$

For tissues that play a role in drug clearance, intrinsic clearance must be included in the equation (Equation 2) (Holt *et al.*, 2019).

$$Vt\frac{dCt}{dt} = (Q \; x \; Cbi - \frac{Q \; x \; Ct \; x \; Rbp}{Kp} - CLint\left(\frac{Ct \; x \; fup}{Kp}\right)) \qquad Equation \; 2.$$

The product of intrinsic clearance times the unbound concentration in tissue divided by Kp forms the clearance term. The CL_{int} in the tissue affects only unbound drug. CL_{int} check can be calculated from the summation of all enzymes entered for the tissue with their respective Vmax and Km values (Equation 3).

$$CL_{int} = \sum_{i=1}^{nEnz}\left(\frac{Vmax}{Km+Ct}\right) \qquad\qquad\qquad Equation \; 3.$$

Hydrophilic and larger molecules tend to follow permeability- limited kinetics, where the limiting rate process for absorption is the permeability across the surface area of a membrane. Drug transfer rate into and out of the tissue is calculated by multiplying the surface area of the membrane with the permeability as well as the saturable transport mechanisms for both influx and efflux. Tissue fraction unbound is in equilibrium with the extracellular space (Holt *et l.*, 2019).
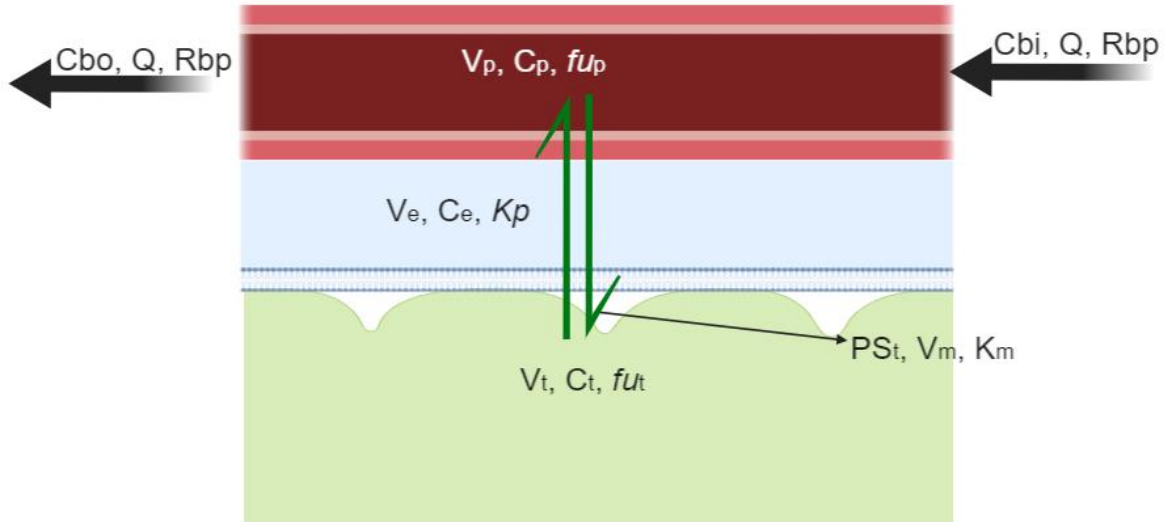
Scheme 2. Schematic view of Permeability – limited tissues.

$$(Ve + Vt\frac{Rbp}{Kp})\frac{dCe}{dt} = Q(Cbi - \frac{Ce \ x \ Rbp}{Kp}) - perm) \qquad \text{\textit{Equation 4.}}$$

$$perm = PSt(Ce - Ct) + V_{influx}(Ce) - V_{efflux}(Ct) \qquad \text{\textit{Equation 5.}}$$

$$Vt\frac{dCt}{dt} = perm - V_{metabolism}(Ct) - Clint(Ct) \qquad \text{\textit{Equation 6.}}$$

Where:

C_e: unbound drug concentration in the extracellular tissue.

$V_{metabolism}$: metabolism rate in the tissue.

V_{efflux}: efflux transport rate from tissue.

V_{influx}: influx transport rate into tissue.

Other parameters are described under perfusion-limited tissues.

Drug transport to the extracellular space is controlled similar to the perfusion-limited model above, with the addition of a permeability term (*perm*) that directs passive entry and exit as well as active influx and efflux to and from the tissue. Tissue concentration change with

respect to time is the total of the passive and carrier-mediated permeability, saturable metabolism, and intrinsic clearance (Chu, 2013).

Key Points in PBPK Model Construction

System-Specific Input Parameters

System-specific parameters (e.g., tissue weight, percent of microsomal protein/ hepatocytes per gram of liver, plasma protein levels and transporter abundance, blood flow, and glomerular filtration rate (GFR)) have been integrated into PBPK models for many species and available by many commercially available software, such as rat, dog, mouse, and human. System-specific parameters to support such models have been utilized widely and are available in the literature (Brown *et al.*, 1997; Jones *et al.*, 2006, 2011, 2013). It is possible to integrate systemic and physiological characteristics to predict different PK parameters and dose in various disease states and population groups (Jones *et al.*, 2013). To predict PK parameters in different populations, we can integrate changes in CYP enzyme expression as well as hepatic blood flow (Q), hematocrit, and liver/renal function (Edginton and Willmann, 2008; Johnson *et al.*, 2010; Yeo and Aarabi, 2011). Many publications supported modeling in different populations such as modeling in geriatrics (Taylor *et al.*, 2009; Chetty *et al.*, 2018), infants and adolescents (Rioux and Waters, 2016; Michelet, 2017; Templeton *et al.*, 2018), pregnancy, fetus and milk transfer (Anderson, 2016; Pfister and Eissing, 2018), obesity (C. Ghobadi, *et al*, 2011), and environmental factors such as smoking (Plowchalk and Yeo, 2012).

Drug-Specific Input Parameters

Drug-specific parameters include drug physicochemical properties such as pKa, basic or acidic, LogP, molecular weight and solubility, and permeability, plasma protein binding (*fup*), blood plasma partitioning [B:P], Kp values and metabolism by hepatic enzymes (Bi *et al.*, 2006; Jones *et al.*, 2012).

Of the important parameters of drug-specific parameters are the Kp values, which are defined as the partition of a drug to the tissue, represented by the movement of the drug into different tissues in the body with the consideration of protein binding and lysosomal trapping (Zhitomirsky and Assaraf, 2015). Kp ratios are usually expressed as the value of the concentration of a drug in a specific tissue to the plasma concentration of the drug at a steady-state (Jones *et al.*, 2006). Many approaches have been used in the literature to define Kp values. Poulin and Rodgers have developed equations to calculate Kp; they assumed that a drug moves and distributes instantaneously and homogenously from plasma to tissue by passive diffusion. The equations to calculate Kp takes into account drug ionization as well as nonspecific drug binding to lipids in the cell membrane and proteins in both plasma and tissues (Berezhkovskiy, 2004; Rodgers and Rowland, 2007; Plowchalk and Yeo, 2012). Poulin and Rogers equations estimates the degree of drug distribution based on the drug's *in-vitro* binding characteristics to lipids and proteins and its physiochemical properties. Equation 7 represents the volume of distribution at steady state (Vss):

$$Vss = \sum(\text{Vt x Kpt}) + \text{Vp} \qquad\qquad \textit{Equation 7.}$$

Where:

Vt: tissue volume.

Kpt: tissue partition coefficient.

Vp: plasma volume.

LogP (o:w) is another input parameter commonly determined for drugs. Compared to LogD that considers both the nonionized and ionized molecules in the aqueous phase, LogP considers only the nonionized species (Poulin and Theil, 2002). The following equation expresses the linear regression analysis from experimental data on LogD and LogP of several organic chemicals (acids, bases, neutrals) (Poulin and Theil, 2002):

$$LogD = 1.115 \ x \ LogP - 1.35 \qquad\qquad\qquad Equation \ 8.$$

Other parameters that are as important are the effective permeability (*Peff*) and the relative *in-vivo* solubility at a certain pH. Caco2 cell lines are usually preferred for permeability measurements. To use the data from Caco2 permeability studies, we need to scale the in-vitro data to *in-vivo* data (e.g., human effective permeability) (Hans Lennernas, 1998). However, measurements of Caco2 (A to B) permeability may under-predict absorption for compounds with high efflux ratios because drug concentrations used in the assay could be lower than the *in-vivo* concentrations, where complete or partial saturation of efflux transporters is probable (Nestorov, 2003). Drug- specific pKa and the pH-partition parameters are usually used to predict the relative solubility of a drug at a certain pH. Drugs that are highly soluble, *in-vivo* data can be used to predict dissolution rate accurately. Unlike drugs that are poorly soluble, where using the *in-vivo* data can under-predict the dissolution rate. Thus, solubility studies in fasted state media simulating the intestinal fluid have been proposed (Jantratid *et al.*, 2008).

Other parameters that can be incorporated into PBPK models include transport-mediated processes. Transporters can be integrated in several tissues if input parameters are available and applicable. These parameters can be obtained from *in-vitro* Caco2 efflux and uptake experiments

in case of intestinal transporters; these parameters can then be spanned to *in-vivo* state by adjusting for surface area (Jantratid *et al.*, 2008).

Routes of Administration

Various routes of administration can be used in the model. The most common dosage routes used are intravenous (IV) and oral (PO). Other routes are sublingual, buccal, subcutaneous (SC), ocular (IO), inhaled, topical, etc. When choosing a route of administration (except for IV), drug dissociation, release, absorption, and distribution from the site of administration should be taken into consideration in the model. Typically, when comparing the built model to data literature, the administration route applied in the model should be the same as the one used in the study (Kuepfer *et al.*, 2016).

PBPK Model Workflow

PBPK models are generated by combining multiple parameters, including the system-specific parameters, drug-specific parameters, and for some cases, drug formulation properties. System-specific parameters, as mentioned above, are related to tissue composition, weight, blood flow, enzymes, and transporters expression levels. These parameters differ depending on the species used or the population of interest. When choosing a particular population, system properties take into account anatomical and physiological changes in that population in relation to the healthy adult reference population. Drug- specific parameters are all parameters related to the drug under study. These parameters are the physicochemical parameters, as mentioned above. By combining the drug-specific parameters and system parameters, a concentration-time profile, and different PK parameters can be predicted (Kuepfer *et al.*, 2016).

After gathering all drug-related parameters, ADME properties and all the system related parameters are adjusted according to the study design and population was chosen, the method for calculation of Kp for different organs are chosen to define the drug distribution behavior. Parameters for clearance can be predicted from plasma concentration-time profiles from *in-vivo* studies. Active transport can be integrated into the model according to the testable hypothesis. Hence, IV data are important in giving us distribution and clearance data regardless of absorption profiles (Center for Drug Evaluation and Research (CDER), 1977).

If reference data are missing or unacceptable, appropriate measures should be taken into account to find existing data in search of a certain physiological data set. If a certain population is being studied, anatomical, biological, and physiological changes in that population group should be used because if not included, it could affect prediction accuracy (Ke *et al.*, 2018*a*). Another example is to take into consideration environmental factors; for example, it has been studied that stress resulting from handling animals affects animals' heart rate, thus increasing cardiac output, eventually leading to variations in resultant PK parameters (Bukowski *et al.*, 1995). In these cases, such an effect should be included in PBPK models. Therefore, physiological parameters exist in connection with model parameters and should be accounted for in PBPK models (Bukowski *et al.*, 1995). In these conditions, allometric scaling (i.e., applied to predict pharmacokinetic parameters such as clearance, volume of distribution, and half-life in pediatrics right from age to age or species to species) can be used to calculate values of physiological parameters that are not available in other sources (Frayer, *et al*; 2005).

Model evaluation should deal with how well the model (predictions) fits the observed data and the hypothesis. In general, a model is evaluated visually by comparing predicted versus observed concentration–time profiles. Furthermore, the general shape of the PK profile, plasma highest concentration (Cmax) and the area under the curve (AUC) should be considered, as well

as the determination of fold change in these parameters (Thiel *et al.*, 2014) (Schwen *et al.*, 2014; Thiel *et al.*, 2014). In addition, other PK parameters like the time to reach the maximum concentration (Tmax), the volume of distribution (V_D), drug clearance (Cl), and the drug half-life ($t_{1/2}$) can be compared between simulated and observed models (Kuepfer *et al.*, 2016).

Another important check for consistency in the model created is model validity over different doses (Jones *et al.*, 2013). If the developed model is for a special population (for example, pregnant women), and if PK parameters are available for that population (pregnant women), the model should be evaluated using these data after changing the specific parameters for that population (for example, pregnant women).

Pharmacodynamic Modeling

Pharmacodynamics (PD) is the study of the effects of drugs and the mechanism of their action on the body. Pharmacodynamic models associate the observed PD "effect" with the plasma concentration or the dose. PD effects can be either therapeutic or toxic. Two types of PD models are available; direct and indirect response models. In the direct response models, the PD response is directly proportional to the plasma concentration of the drug or the unbound fraction in a tissue (f_{ut}) In the indirect response models, the drug effect will happen after the drug redistributes from the central compartment to the "effect" compartment, the true site of the pharmacological effect, which is linked to the central compartment (Wright *et al.*, 2011).

PBPK Modeling and Simulation in Drug Research and Development

Throughout drug discovery and development, data from a drug candidate such as ADME properties or data from *in-vitro* and *in-vivo* experiments are used to predict different PK parameters in various populations and in DDI, which will assist in choosing the best drug

candidate. Recently, pharmaceutical companies have increased funding for drug metabolism and pharmacokinetics (DMPK) studies at nearly every stage of the drug discovery process (Metabolism *et al.*, 2000; Kwon *et al.*, 2004). Though, enhancements in models and predictions of drug distribution, hepatic clearance and several more have granted PBPK models to be accomplished without the need for any *in-vivo* data. PBPK models provide an exceptional structure to integrate all of the accessible data for drugs and to assure more accurate predictions of the numerous outcomes under exploration in a human physiological context. The knowledge obtained from PBPK simulations can be used to lead drug development, and drive to enhanced efficiency and reduced costs. Such enhancements are suitable when one or more of the PK-determining parameters is in the 'blind spot' (i.e., in the range of values for a parameter in which no clear conclusions can be drawn regarding their impact *in-vivo*) (Lipscomb *et al.*, 1998).

Applications of PBPK Modeling

There are many applications to PBPK modeling, including drug simulation in healthy subjects as well as different populations. PBPK modeling can also be used for preclinical simulation, to predict DDI and to predict the effect of changes in absorption, formulation, and food on drug exposure. Because there is a variety of PBPK applications, the affiliation of experts from a range of backgrounds, including formulation scientists, pharmacometricians, clinical pharmacologists, clinicians, and statisticians, is important to ensure a fulfilled implementation and application of PBPK modeling and simulation in drug discovery and development.

Drug-Drug Interactions

Patients with concurrent diseases are usually exposed to polypharmacy. Drug co-administration increases the risk of drug-drug interactions (DDI). Drug interactions can alter PK parameters and ADME properties of a drug due to co-administration of another drug, which is frequently due to induction or inhibition of enzyme and/or a transporter (Varma *et al.*, 2015). Drug interactions can lead to adverse effects, toxicity, or it may affect drug efficacy (Zhang *et al.*, 2009). Consequently, models have been developed to predict several DDI and changes in PK parameters with drug co-administration (Boulenc and Barberan, 2011).

Several methods are used to define DDI; the first approach is called the [I]/Ki approach; this model describes the alteration in drug exposure in the presence of an inhibitor. It is usually expressed as:

$$AUCi/_{AUC\ control} = 1 + [I]/Ki \qquad\qquad\qquad Equation\ 9$$

Where:

AUC: is the area under the curve in the presence (i) and in the absence (control) of the inhibitor drug.

[I]: is the *in-vivo* inhibitor concentration.

Ki: the inhibition constant.

Assumptions are made in this method, where this model assumes the drug cleared mainly via one metabolic pathway that is primarily affected by the inhibitor. It also assumes that the drug is not metabolized in the intestine at all (Einolf, 2007).

The second approach is called the mechanistic static model (MSM) where the substrate is presumed to be metabolized in both the liver and the intestines so the net effect of the inhibition or induction is all incorporated in the model and the fraction metabolized (*fm*) of the substrate drug is considered. The limitation of this model is that it takes into consideration the inhibitor

concentration; therefore, the magnitude of AUC change is based on the inhibitor concentration (Fahmi *et al.*, 2008).

The latter approach is the mechanistic dynamic models (MDM), which describes the time- variable concentrations of the inhibitor. It takes into account factors such as CYP expression, genetic polymorphisms, intestinal metabolism, etc., and the ability to consider hepatic uptake (Nordmark *et al.*, 2014).

Modeling in Infants and Pediatrics

Drug studies in this population are limited for many reasons including only children who will benefit from the study can participate, blood collections are harder in infants than adults, and liquid drug formulation should be offered or a smaller pill size (Verscheijden *et al.*, 2019). One important feature to consider is physiological differences between adults, children, and infants (organ size, weight, blood flow, and enzyme and transporter abundance), thus, making dose prediction hard in this population.

Generally, dosing in the pediatric population has always been developed based on adult dosing schedule (after adjustments for weight or body surface area (BSA)) or by using allometric scaling (Mahmood, 2014). However, many variances have been recognized between adults, pediatrics, and infants. Some of these differences are: variations at the absorption level, drugs are typically absorbed at a slower rate in infants than in adults, resulting in longer Tmax. In addition, stomach acidity is lower in younger children, and that will result in faster absorption of weakly acidic drugs (Templeton *et al.*, 2018). At the distribution level, plasma proteins exist at a much lower concentration in pediatrics than adults, which results in the higher free fraction of drug in pediatrics (especially for highly protein-bound drugs) (Mcnamara and Alcorn, 2002). Intracellular and extracellular water levels are higher in infants compared to adults. Therefore,

water-soluble drugs will possess a larger volume of distribution in pediatrics than adults (Templeton *et al.*, 2018). Enzymatic activity is higher in adults than pediatrics (30–70 % of that in adults), resulting in a slower elimination rate in pediatrics (Verscheijden *et al.*, 2019). Besides hepatic metabolism, pediatrics GFR is about 60% of adult values, and because of an increase in renal blood flow, GFR increases rapidly in the first 2 weeks of life, until adults values are reached at the age of 12 months of age (Mahmood, 2014; Loebstein and Koren, 2016).

Modeling in Geriatric Population

Even though it is the largest population to receive medications, they are not usually involved in clinical trials due to organ function variability and the existence of polypharmacy. Many of the system-specific parameters are affected with age; height and weight are also likely to decrease with age (Schlender *et al.*, 2016). A decrease in cardiac output results in decreased organ blood flow (Bolomey *et al.*, 1949). No significant change in plasma protein concentrations have been noticed with age (Campion, 1990*a*, *b*). Several studies have investigated changes in CYP enzymes with age, but no age-related changes in activity have been published except with CYPs 1A2, 2D6, and 2E1, which is shown to decrease with age, with more than 25% (Parkinson *et al.*, 2004). PBPK modeling will be useful in geriatrics where it could predict DDI where patients are usually on polypharmacy.

Modeling in the brain and the central nervous system (CNS)

Drug penetration into the brain is primarily limited by the blood-brain barrier (BBB), due to the existence of tight junctions as well as active efflux and uptake transporters at this barrier. The prediction of brain concentrations is regulated by a) the tight BBB and blood-CSF barrier (BCSFB), which controls the passage of drugs from the systemic circulation to the brain (Lange,

2013). These barriers are associated with limited passive diffusion; and b) physiological flows, including the microvascular blood flow that facilitates central nervous system (CNS) drug concentrations (Liu *et al.*, 2005).

Several PBPK models for BBB drug distribution have been published, yet we do not have any model that predicted drug concentrations in the human CNS (Liu *et al.*, 2005; Badhan *et al.*, 2014; Dedrick, 2019). Testing a drug's brain concentration is nearly impossible. Therefore, the importance of brain PBPK models being used. However, it is still limited as CSF sampling of drug concentration is unlikely to be feasible or ethical, and sometimes, CSF drug levels do not represent brain levels. Several physicochemical properties could determine a drug's ability to cross the BBB, including molecular weight, lipophilicity, ionization constant, fraction unbound in plasma, partitioning to the brain, and whether it is a transporter substrate or not. A mixture of drug-specific properties such as permeability properties, transmembrane transport of drugs as well as the surface areas of the BBB control the transport of drug through the BBB. Transport proteins such as P-glycoprotein (P-gp), multidrug resistance-associated protein (MRPs), organic anion transporters (OATs), and organic anion transporting polypeptides (OATPs) could also mediate the active transport of drugs (Westerhout *et al.*, 2011).

Modeling in pregnancy and fetus exposure

Pregnant women define a distinctive population when it comes to drug administration. Although drug use in the pregnant population is common and rising, pregnant subjects are usually banned from joining clinical trials due to legal, ethical, and practical causes. This results in limited PK information in the pregnant population. Major physiological and anatomical changes occur during pregnancy, including weight, organ blood flow, GFR, and changes in the activity of metabolizing enzymes, which could alter PK of drugs. Conversely, due to the lack of

PK data in pregnant women, data are usually obtained by extrapolation from non- pregnant to pregnant subjects, risking either sub-therapeutic drug levels or toxic levels on the mother and the fetus.

Because it is challenging to acquire PK data for drugs from *in-vivo* studies, pregnancy PBPK models are considered a favorable method to create vital understandings into the PK of drugs, and this can consequently be used to explain and lead clinical studies in pregnant women, especially with respect to suitable dosing.

Caffeine

Caffeine (1,3,7-trimethylxanthine) is an alkaloid with a chemical composition of $C_8H_{10}N_4O_2$ and a molecular weight of 194.19. Besides its biological existence in some foods, caffeine is added to food and used as a drug or a constituent of many pharmaceutical formulations. Caffeine is water soluble (solubility of 13.92 mg/ml) but it is lipophilic enough to passively cross membranes (LogP -0.15); it is also a weak base with a pKa of 2.24, which makes it more in the unionized form at the intestinal absorption layer, thus it is easily absorbed. It is the most commonly used psychostimulant or CNS stimulant in the world (Insler, 2014). It has multiple pharmacological and physiological effects, including cardiovascular, renal, respiratory, and smooth muscle effects, in addition to effects on mood, memory, alertness, and physical and cognitive performance (Tang-Liu *et al.*, 1983).

Due to the fact that caffeine metabolism rate is low in the fetus due to low levels of metabolizing enzymes mainly CYP1A2, caffeine clearance is prolonged in pregnant women. In addition, Caffeine may also influence cell function through increasing cyclic adenosine monophosphate (cAMP) concentrations and it causes and increase in the circulating catecholamines (mainly epinephrine). Therefore, higher caffeine doses could lead to miscarriage.

The study of PK of a drug in pregnant women is unethical and unfeasible, so using PBPK

modeling help us understand how a drug acts in pregnant women, where all the anatomical and

physiological changes happen.

5-HT3 receptor antagonists

There are varieties of highly selective and effective compounds that antagonize 5-HT3

receptors. The 5-Hydroxytryptamine 3 (5-HT3) receptor is a ligand-gated ion channel, and it is

anatomically and mechanically distinctive from the other 5-HT receptors who present their effect

through G-proteins. 5-HT3is able to facilitate fast excitatory neurotransmission in the CNS and

peripheral nervous system (PNS) (Sugita *et al.*, 1992). 5-HT3 receptors are distributed in many

brain regions, with the highest levels of distribution in the brainstem, especially in regions

associated with the control vomiting and reflux, such as the area postrema (AP). The existence of

5-HT3-binding sites in the CNS was first recognized using a radiolabeled 5-HT3 receptor

antagonist ([3H]GR65630) (Kilpatrick *et al.*, 1987; Tecott *et al.*, 1993). 5-HT3 receptors also

control gut motility, secretion, and peristalsis (Galligan, 2002; Engel *et al.*, 2013). 5-HT3

receptor antagonists share a basic amine, a rigid aromatic or hetero-aromatic ring system, and a

carbonyl group, and there are marginally longer distances between the aromatic and amine group

when compared to the agonist pharmacophore (Schmidt and Peroutka, 1989). Additional work

has revealed that 5-HT3 receptor can only handle minor substituents on the charged amine such

as a methyl group (Schmidt and Peroutka, 1989). To be a potent antagonists for the 5-HT3

receptors, a compound should have 6, 5 heterocyclic rings, where the presence of the 6

membered aromatic ring gives it the highest potency (Schmidt and Peroutka, 1989).

Many studies characterized the 5HT3 receptor using the nonselective compounds

morphine and cocaine (GADDUM and PICARELLI, 1957; Kilpatrick, 1990). Using serotonin as

the source, bemesetron and tropisetron were formulated. Nowadays, many 5- HT3 receptor antagonists are in clinical use, which includes tropisetron, ondansetron, granisetron, dolasetron, palonasetron and zacopride (the latter, acting at nanomolar concentrations) (Lummis, 2012). These drugs have been extensively used for the treatment of chemotherapy-induced nausea and vomiting in cancer patients (CINV) or nausea and vomiting from radiation therapy (Lovinger, 1991).

Granisetron

Granisetron is an azabicyclic compound, a selective 5-hydroxytryptamine (5-HT3) receptor antagonist, which does not act on 5-HTIA-D, 5-HT2, 5-HT4, dopamine Dl or D2, histamine HI, benzodiazepine or αl, α2 or adrenergic receptor binding sites. Because of its antiemetic and anti nauseant effects, granisetron is widely used to treat CINV (Plosker and Goa, 1991; Yarker *et al.*, 1994). Granisetron is a basic compound with a pKa of 9.21 which makes it mainly ionized at the absorption site. It has a LogP of 2.2 which makes it lipophilic with a relatively good solubility of 17 mg/ml.

Granisetron most likely employs its actions on acute emesis (i.e., episodes arising within 24 hours of cytotoxic therapy) by acting at both peripheral vagal nerve and central vomiting sites. In the periphery, it prevents serotonin-induced stimulation of vagal afferent nerves in the gastrointestinal tract; centrally, it prevents the stimulation of 5-HT3 receptors in the chemoreceptor trigger zone (CTZ) in the brain stem, which activates the vomiting reflex (Nayak *et al.*, 1999).

The pharmacokinetic profile of granisetron has been evaluated in healthy volunteers. Granisetron poses a large volume of distribution (Vd) of nearly 250L in healthy subjects (Roche, 2013). Since the pharmacokinetics of granisetron is linear, peak plasma concentrations (Cmax)

and the area under the plasma concentration-time curve (AUC) increase proportionally with dose, while elimination half-life ($t_{1/2}$) and total plasma clearance (Cl) persist unaffected. The $t_{1/2}$ has been calculated to be around 3 to 4 hours, and the Cl is between 33 and 51 L/h (R., 1994; Roche, 2013).

Granisetron is cleared mainly by hepatic metabolism, with less than 20% of the dose eliminated unchanged in the urine. Granisetron is metabolized mainly by the cytochrome P450 1A2 subfamily, established by ketoconazole inhibition studies *in-vitro* in liver microsomal studies (Roche, 2013). The predominant form of this enzyme subfamily is 3A4 (Baldwin *et al.*, 1999), and, unlike CYP2D6, polymorphisms of the CYP3A subfamily have not been demonstrated (Davis and Homsi, 2001). CYP450 inducers or inhibitors may affect the clearance and, hence, the half-life of granisetron.

The pharmacodynamic effects of 5-HT3 receptor antagonists differ among drugs. Granisetron poses the highest selectivity and superior affinity, as studied *in-vitro* (Nayak *et al.*, 1999). Granisetron has shown to be effective in controlling CINV. However, some patients still suffer from nausea and vomiting following chemotherapy. We aimed to study the reason for this variability in the granisetron effect. In order to study that, we applied PBPK models to predict the effect of transporter (P-gp) and lysosomes on granisetron permeability. We also used PBPK models to predict the effect of genetic variations in CYP enzymes on granisetron plasma and brain levels.

Study objectives

        In my work, I used PBPK modeling using GastroPlus™ software to evaluate the effect of changes in drug-metabolizing enzymes and transport proteins on drugs PK and PD in different populations and physiological conditions as follows.

Chapter 2 objectives (Caffeine):

1- To assess the relationship in changes in caffeine PK parameters on PD parameters related to miscarriage

2- To verify and extend previously developed PBPK models for caffeine in the pregnant population to predict changes in caffeine PD parameters associated with miscarriage risk.

Chapter 3 objectives (Granisetron):

1- To identify the effect of P-gp and lysosomal entrapment on granisetron intestinal permeability and plasma profiles following oral dosing.

2- To develop a PKPD model to validate and predict the effect of genetic variations in CYP1A1 and CYP3A5 on granisetron levels in plasma and brain, and predict the effect of these genetic variations on the occupancy of 5-HT3 receptors.

Chapter 2

Physiologically Based Pharmacokinetic/ Pharmacodynamic Model for Caffeine Disposition in

Pregnancy

Abstract

Caffeine is the most consumed active stimulant and about 80% of pregnant women consume caffeine orally on a daily basis. Many reports indicate consumption of >200 mg per day caffeine during pregnancy could increase the likelihood of miscarriage. In this paper, we developed a physiological based pharmacokinetic/pharmacodynamic (PBPK/PD) model for caffeine in pregnancy to examine the association between maternal caffeine consumption and caffeine plasma levels at doses lower and higher than 200 mg, the goal of this effect is to predict changes in caffeine concentrations across the 3 trimesters, and to predict associated changes in caffeine PD parameters. Two models were successfully developed using GastroPlus™ software, a non-pregnant model for validation purposes, and a pregnant model for validation and prediction of maternal caffeine plasma concentrations following single and multiple dosing. Using observed and predicted data, we were able to validate and simulate PK changes of caffeine in non-pregnant women and the PD effect of caffeine on certain enzymes and catecholamines associated with caffeine intake. Furthermore, the pregnancy PBPK model successfully predicted changes in caffeine PK across the three trimesters. Caffeine increased exposure during pregnancy was related to reduced activity of caffeine metabolizing enzyme CYP1A2. The model also predicted increased levels of caffeine in the fetoplacental compartment (FPC) due to increased maternal caffeine plasma concentrations. Increased caffeine levels in maternal blood was accompanied with greater inhibition of phosphodiesterase enzyme, higher cyclic adenosine monophosphate and a greater increase of epinephrine levels, which could increase the risk of pregnancy loss. The application of the developed PBPK model to predict PD effect could provide a useful tool to help define potential cut-offs for caffeine intake in various stages of pregnancy.

Introduction

Caffeine is one of the most ingested substances in the world. It is found in many beverages such as coffee, tea, soft drinks, and chocolate at different concentrations (Knight *et al.*, 2004). Caffeine consumption is generally associated with a large number of diseases and health alterations. In humans, caffeine may affect the heart by increasing blood pressure, central nervous system by increasing anxiety, and the respiratory system by affecting the regulation of breaths, which are mainly caused by caffeine effect on adenosine receptor A1 (Rieg *et al.*, 2005; Umemura *et al.*, 2006; Echeverri *et al.*, 2010).

Caffeine is extensively metabolized by the enzyme CYP1A2 to 1, 7-dimethylxanthine by N-3 demethylation; it also generates other metabolites like theobromine and theophylline with only 3% of the dose excreted unchanged in the urine (Tang-Liu *et al.*, 1983). Caffeine is rapidly absorbed from the digestive tract with a bioavailability of almost 100% (Blanchard, 1983)(Blanchard, 1983) . It distributes throughout all tissues, freely crosses the placenta to the fetus, and has been detected in the amniotic fluid and umbilical cord (Avram Goldsten, 1961). It is estimated that 70-80% of pregnant women utilize some caffeine daily (Li *et al.*, 2015*a*). The average daily consumption of caffeine from caffeine sources was estimated at around 106-170 mg per day for adults and 58 mg per day for pregnant women (Aldridge, *et al*, 2005). The half-life of caffeine in non-pregnant subjects is between 1.5 and 10 hours (Knutti *et al.*, 2014), whereas in pregnant women, it increases up to 18 hours in the third trimester (Knutti *et al.*, 2014). The effect of caffeine on the outcome of pregnancy have been reported in many studies (Aldridge, *et al*, 2005; 'Theophylline, 2001.; John R.Giudicessi, BA.Michael J.Ackerman., 2008; Gaohua *et al.*, 2012; Isoherranen and Thummel, 2013; Ke *et al.*, 2014; Knutti *et al.*, 2014). Drug pharmacokinetics (PK) are often altered during pregnancy (Ke *et al.*, 2014; De Sousa Mendes *et*

al., 2015; Colbers *et al.*, 2016; Jogiraju *et al.*, 2017), which makes it necessary to modify the usual doses of drugs for pregnant women. In pregnancy, CYP1A2 activity is decreased throughout pregnancy by 32.8% in the first trimester (T1), 48.1% in the second trimester (T2) and 65.2% in the third trimester (T3) (Tracy *et al.*, 2005), suggesting caffeine clearance is prolonged in pregnant women. In addition, caffeine metabolism rate is low in the fetus due to low levels of metabolizing enzymes (Infante-Rivard *et al.*, 1993). Caffeine may also influence cell function through increasing cellular cyclic adenosine monophosphate (cAMP) concentrations (Echeverri *et al.*, 2010; Montoya *et al.*, 2014), and decreases intervillous placental blood flow via increasing circulating catecholamines mainly epinephrine (Kirkinen *et al.*, 1983*a*). Therefore, caffeine could have an adverse effect on fetal development (Li *et al.*, 2015*a*).

Caffeine intake has been reported to increase the risk of miscarriage (Claire, 1993; Pollack *et al.*, 2010, Li *et al.*, 2015*b*; Okubo *et al.*, 2015; Rhee *et al.*, 2015). Thus, maternal caffeine intake during pregnancy has attracted significant attention with regard to its possible effects on birth outcomes and miscarriages. Findings from epidemiological studies in pregnant women suggested caffeine intake in pregnancy of more than 300 mg per day could increase the risk of spontaneous abortion (COT Statement, 2001; Okubo *et al.*, 2015). In addition, both the World Health Organization (WHO) and the European Food Safety Authority reported caffeine consumption up to 300 mg/day and 400 mg/day, respectively, does not give rise to safety concerns for non-pregnant adults, and caffeine consumption up to 300 or 200 mg per day, respectively, by pregnant women does not give rise to safety concerns for the fetus (EFSA, 2015; WHO, 2016). Pregnant women whose caffeine intake is more than 200 mg/day have a much greater risk of miscarriage compared to those who consume less than that (Rhee *et al.*, 2015). Higher caffeine consumption was associated with a higher risk for both early and late

miscarriage; however, the association appeared to be more for later than earlier miscarriage (Rhee *et al.*, 2015).

Interest in applying physiologically based pharmacokinetic/pharmacodynamic (PBPK/PD) modeling in pregnancy is growing. Several reports have been published describing PBPK/PD models' development to simulate and predict dosing regimens and drugs disposition in pregnant women (Tracy *et al.*, 2005; Gaohua *et al.*, 2012; Xia *et al.*, 2013; Alqahtani and Kaddoumi, 2015; De Sousa Mendes *et al.*, 2015; Colbers *et al.*, 2016; Jogiraju *et al.*, 2017, Ke *et al.*, 2018*a*). In addition, several studies reported the development of PBPK models to evaluate the effect of pregnancy-associated changes in CYP1A2 activity on caffeine kinetics in pregnant women using different software including Simcyp, PK-Sim and MoBi (Gaohua *et al.*, 2012; Partosch *et al.*, 2015; Dallmann *et al.*, 2018). However, studies to simulate or predict the effect of increased levels of caffeine, due to reduced levels of CYP1A2, on caffeine PD in pregnancy are yet to be achieved. Studies that used pharmacokinetic parameters to predict pharmacodynamic parameters are not yet available. Thus, in the current study, using GastroPlus™ software, we aimed to assess the relationship in changes in PK parameters on PD parameters related to miscarriage so we can predict cutoffs of caffeine intake for each trimester. We also aimed to verify and extend previously developed PBPK models for caffeine in pregnant population to predict changes on caffeine PD parameters associated with miscarriage risk by performing the following: 1) develop and validate a non-pregnancy and pregnancy PBPK/PD models that consider the physiochemical and PK of caffeine, and physiologic and metabolic changes that normally occur during pregnancy, 2) validate and predict PK changes of caffeine across the three trimesters of pregnancy and the PD effect of caffeine on certain enzymes and catecholamines associated with caffeine intake, and 3) predict potential cut-offs for caffeine

intake in various stages of pregnancy to avoid reported an increased risk of miscarriage with high

caffeine intake.

Experimental Section

Software and Workflow of PBPK Model and Model Validation

All simulations were performed using the software GastroPlus™ (Version 9.5; Simulation Plus Inc., Lancaster, CA) integrated with ADMET Predictor, and PBPKPlus™ and PDPlus™ modules. The general workflow of caffeine PBPK model development and validation consisted of the following steps. First, the PBPK model was initially developed using the physicochemical, biopharmaceutical, and pharmacokinetic parameters obtained from the literature (Cheng *et al.*, 1990; Birkett and Miners, 1991), or estimated by ADMET Predictor in non-pregnant women population (Table 1). The model was further validated by comparing the simulated PK data from a virtual population with the observed clinical studies. Second, in case that predicted PK profile and parameters were deviant from the observed data, the model was refined by parameter optimization by fitting against the non-pregnant clinical data. Third, the pregnancy PBPK model was developed with these verified drug-specific parameters and pregnancy-induced physiological changes. Population-dependent physiological parameters for non-pregnant and pregnant PBPK models were obtained using the Population Estimates for Age-Related Physiology™ module in GastroPlus™ with a size of 25 virtual female subjects (chosen randomly by the software) per population with an average age from 20 to 40 years old. The predicted mean values of the PK parameters C_{max} (plasma highest concentration) and AUC (area under the curve) for non-pregnant and pregnant women were then obtained based on the simulations. The predicted mean values of the PK parameters C_{max} and AUC for non-pregnant and pregnant women, as well as these parameters ratios, were then obtained based on the simulations. Besides C_{max} and AUC, verification of the established PBPK models was based on the time at which the

39

drug presents the highest concentration (T_{max}), volume of distribution (V_d), systemic clearance

(Cl), and half-life ($t_{1/2}$).

Table 1. Physiochemical and pharmacokinetic parameters of caffeine used in PBPK model.

Parameter	Value	Reference
Molecular Weight (g/mol)	194.19	[a]
LogP	-0.15	[a]
Ionization constant (pKa)	2.24 (base)	Estimated by ADMET predictor
Bioavailability (%)	100	[b]
Blood/plasma ratio (Rbp)	1.03	Estimated by ADMET predictor
Solubility at pH 7.4 (mg/ml)	13.92	Estimated by ADMET predictor
Diffusion Coefficient (cm^2/s)	1.037×10^{-5}	Estimated by ADMET predictor
Fraction unbound (f_u)	0.7	Estimated by ADMET predictor
CYP 1A2 Vmax (mg/sec)	0.00759	[c]
CYP 1A2 Km (mg/l)	8.46	[c]
Renal clearance (l/h)	0.00246	[d]
V_d (l/kg)	0.51	[e]

[a] drugbank.ca; https://www.drugbank.ca/drugs/DB00201
[b] Bioavailability taken from reference [Blanchard, 1983].
[c] Optimized values from in vitro taken from reference [(Grant *et al.*, 1987)] (reported values were 0.006 mg/sec
    for Vmax and 8.1 mg/l for Km).
[d] Renal clearance was taken from reference (Birkett and Miners, 1991).
[e] V_d; Volume of distribution was taken from reference (Cheng *et al.*, 1990).

Two models were thus developed, non-pregnant and pregnant models. Three different doses of caffeine were tested in the non-pregnant model and over the three trimesters in the pregnant model. The PBPK models represent the organs that are relevant to drug absorption, distribution, excretion, and metabolism (ADME). These organs are heart, lung, brain, gut, spleen, gut, liver, kidney, adipose tissue, muscle, skin, and reproductive organs. The tissues are linked by the arterial and venous blood, and each compartment has its own blood-flow rate, volume, and tissue-partition coefficient (Kp) (Alqahtani, *et al*, 2015)). Default values of Kp implemented in GastroPlus were used, which were calculated using the tissue composition equations according to the relationship between physiological data and compound-specific determinants of distribution like lipophilicity (LogP), ionization (pKa), and plasma protein binding (fu). The Kp value for the fetoplacental unit was assumed to have similar Kp value for the brain: plasma partition coefficient; this assumption was mainly based on their similar characteristics, such as high blood perfusion and the existence of blood-tissue barriers (Gaohua *et al.*, 2012) (Alqahtani, *et al*, 2015). Kp values used in the non-pregnant and pregnant (T3) models are listed in Table 2; Kp values used for T1 and T2 models were close to T3 values. The plasma protein binding (fu) value was assumed not to change by pregnancy, which is consistent with other reports (Dallmann *et al.*, 2018), and thus the same fu value of 0.7 was used in the non-pregnant and pregnant models across the 3 trimesters. Organs were also assumed to be perfusion rate-limited in both pregnant and non-pregnant models. The liver and kidney were considered to be the only organs to eliminate caffeine.

Following models development and validation, PDPlus™ module was used to validate observed data and predict PD data over trimesters for phosphodiesterase (PDE), cAMP, and epinephrine.

Development and Validation of PBPK Model in Non-Pregnant Subjects

Physiochemical and PK parameters of caffeine used in the PBPK model are presented in Table 1. Concentration-time profiles from healthy women were used, and a population PBPK model for non-pregnant was built and then validated using data from the literature (Cheng *et al.*, 1990), by scanning with GetData Graph Digitizer (version 2.26; http://getdata-graph-digitizer.com). Physiological values for intestinal volumes, lengths and pH in humans used were those built in the software, except for the stomach transit time, which was changed from 0.25 h to 0.1 h because the model was developed for caffeine administered as an oral solution (Parrott *et al.*, 2014)

Table 2. Default values in GastroPlus of Tissue-to-Plasma Partition Coefficients (Kp) of caffeine used in non-pregnant and pregnant (T3) subjects PBPK models.

Tissue	Non-pregnancy	Pregnancy
Lung	0.2	0.21
Adipose	0.32	0.32
Muscle	0.06	0.06
Spleen	0.1	0.1
Heart	0.17	0.12
Liver	0.51	0.5
Kidney	0.14	0.14
Skin	0.29	0.27
Brain	0.51	0.601
Red bone marrow	0.1	0.1
Yellow Bone Marrow	0.05	0.05
Rest of Body	0.06	0.06
Reproductive organ (Fetoplacental Unit)[*]	0.15	0.601

[*] Assumed to be similar to brain value.

Caffeine is mainly metabolized by CYP1A2. Liver metabolism was considered in the simulation by using in vitro K_M and V_{max} values for CYP1A2 reported in the literature that were optimized by GastroPlus to fit caffeine plasma profiles better and predict clearance (Grant *et al.*, 1987; Ke *et al.*, 2013) Optimized values used for K_M is 8.46 mg/l (reported 8.1mg/l) (Grant, D, 1987) and for V_{max} is 0.00759 mg/sec (reported 0.006 mg/sec) (Grant *et al.*, 1987), (Table 1). Caffeine is a water soluble compound but sufficiently hydrophobic to pass through tissue membranes (Grant *et al.*, 1987); thus perfusion-rate limited kinetics were used in the simulation expressed in this equation:

$$Vt\frac{dCt}{dt} = Q * Cbi - \frac{Q * Ct * Rbp}{Kp} - CLint\left(\frac{Ct * fup}{Kp}\right)$$

Where Cbi = blood concentration in arterial; Rbp = blood/plasma concentration ratio; Vt = tissue volume; Cv, Ct = plasma and tissue concentrations; Kp = tissue/plasma partition coefficient; *fup* = fractions unbound in plasma; CL_{int} = Tissue intrinsic clearance.

Development and Verification of PBPK Model in Pregnant Women

We simulated caffeine PK in pregnant women using a PBPK model with the same organs mentioned in non-pregnant subjects but substituting the reproductive organ (a default in GastroPlus™ PBPKPlus module) with the fetoplacental compartment (FPC). FPC represents the intra-uterine components, including the fetus, placenta, amniotic fluid and uterus (Abduljalil *et al.*, 2012, Ke *et al.*, 2018*a*, *b*). The compartment of the fetoplacental units was also assumed to be perfusion rate limited. Pregnancy PBPK model was developed with verified drug-specific parameters, similar to those used in the non-pregnant model, and pregnancy induced physiological changes such as changes in cardiac output, weight, hematocrit, blood flow and the volume of the fetoplacental compartment changes along with

progressing in trimesters of pregnancy as shown in Table 3 and Figure 1. Caffeine

accumulation over the three trimesters was tested; the average of each trimester (average

T1=6 weeks, average T2=25 weeks, average T3=35 weeks) was applied in the equations

presented in Table 3 to obtain pregnancy induced physiological, anatomical and biological

changes that were used as input parameters in GastroPlus™. Gut physiology was assumed to

be the same in non-pregnant and pregnant subjects (Xia, B.; 2013 and Alqahtani ,*et al*, 2015)

The decrease in CYP1A2 activity for each trimester was added to the model (i.e. by 32.8% in

first trimester, 48.1% in second trimester and 65.2% in the third trimester) (Tracy et al, 2005).

The cardiac output increased by 18, 28 and 30% in the first, second, and third trimester of

pregnancy (Abduljalil *et al.*, 2012). In addition, uterine blood flow significantly increased

from 0.5% of cardiac output in non-pregnant women to 12% in late pregnancy (Abduljalil *et*

al., 2012)

Table 3. Physiological, anatomical and biological changes that occur during pregnancy. Regression equations needed for p-PBPK model during different gestation ages (GA) in weeks, based on Abduljalil *et al*.

Parameter	Equation
Total body weight (TBW) (kg)	TBW = 61.1+0.2409 GA +0.0038 GA2
Cardiac output (CO) (l/min)	CO = 301+5.916 GA−0.088 GA2
Hematocrit (Hct) (%)	Hct = 39.1–0.0544 GA—0.0021 GA2
Uterine blood flow (l/h)	Uterine blood flow = 1.71+0.2068 GA+0.0841 GA2−0.0015 GA3
CYP1A2 activity (%) – Frist Trimester	Decreased by 32.8%
CYP1A2 activity (%) – Second Trimester	Decreased by 48.1%
CYP1A2 activity (%) – Third Trimester	Decreased by 65.2%
Fetoplacental volume = Uterus weight + Placenta volume + Fetal volume + Amniotic fluid volume	
Uterus weight (g)	Weight of the uterus = 80+8.2931 GA+0.3546 GA2
Placenta volume (ml)	Placenta volume = 0.0−0.0716+0.9146 GA2−0.0122 GA2
Fetal volume (ml)	Fetal volume = 0.01 exp(13.604(1−exp(−0.0702GA)))
Amniotic fluid volume	Amniotic fluid volume = 0+1.9648 GA−1.2056 GA2+0.2064GA3−0.0061 GA4+0.00005 GA5
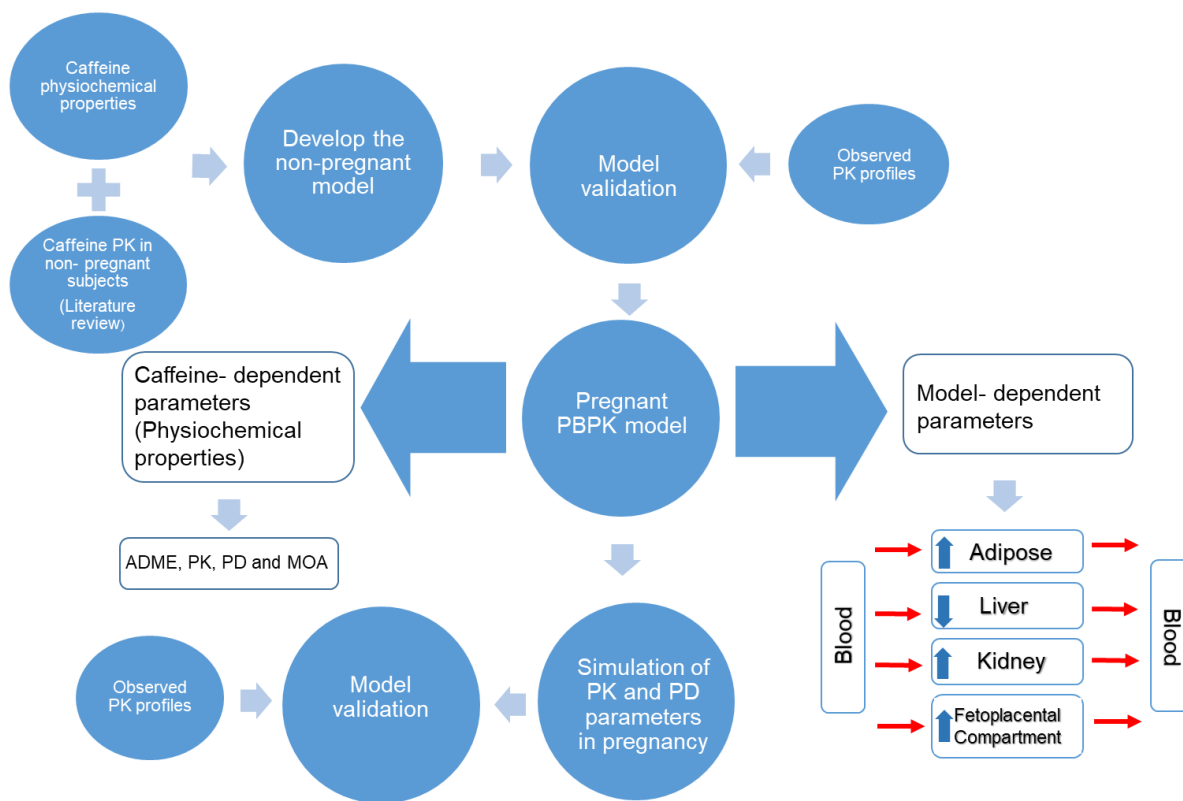
Figure 1. Structure of pregnancy physiologically based pharmacokinetic (p-PBPK) model.

Pharmacodynamic Model

Many studies have found a relation with caffeine intake and miscarriage (Infante-Rivard *et al.*, 1993; Weng *et al.*, 2008; Pollack *et al.*, 2010; Jahanfar S, 2015, Li *et al.*, 2015*b*; Okubo *et al.*, 2015) Pregnant women who consume caffeine intake more than 200 mg per day have a greater risk of miscarriage compared to those who consume less than 200 mg per day (Weng *et al.*, 2008). Caffeine plays a role in cell division through inhibition of PDE (Montoya *et al.*, 2014), which triggers a rise in cellular cAMP (Montoya *et al.*, 2014), and thus epinephrine that causes uterine contractility and sometimes miscarriage (Montoya *et al.*, 2014).

Built-in PD modules in GastroPlus™ were used. Direct and indirect PD models were fitted to concentration-time and PD effect-time profiles for high (618 mg) and low (179 mg) caffeine doses, reported in the literature (Kirkinen *et al.*, 1983*a*, *b*). to find best model to describe

relationship between maternal concentration-time profile and PD effect of caffeine. For caffeine

effect on PDE, it is an inhibitory process and presented as an indirect module in GastroPlus™.

Thus, the built-in PD indirect module with the effect was used as presented in the following

equation:

$$I = 1 - \frac{Imax\ C}{IC50 + C}$$

Therefore:

$$\frac{dR}{dt} = kin\left(1 - \frac{ImaxC}{IC50 + C}\right) - koutR \quad 0 \leq Imax \leq 1$$

Where ImaxC is the maximal inhibitory concentration, IC50 is the concentration of an inhibitor

required to reduce the rate of an enzymatic reaction by 50%, kin and kout represent rate

constants for drug transfer from plasma to effect compartment and from effect compartment to

plasma, respectively, and R is the rate of generation and dissipation of the response in the

absence of the drug.

For caffeine effect on cAMP and epinephrine, PD response is directly proportional to

caffeine concentration. Effect is presented in the following equation:

$$E = E0 + \frac{EmaxC}{EC50 + C}$$

Where *E0* is the baseline response, Emax is the maximum response, C is drug concentration and

EC50 is the concentration at which 50% of the maximum response is observed.

Results

Development and Validation of PBPK Model in Non-Pregnant Subjects

Input data that were used in the simulation are presented in Table 1. Concentration-time plasma profiles from healthy women were used to construct and validate the PK model for non-pregnant women (Cheng *et al.*, 1990). The model was developed and validated against the disposition kinetics for 3 different doses of caffeine at 70, 200 and 300 mg (Cheng *et al.*, 1990). The simulated plasma concentration-time profiles captured the observed PK profiles (Figure 2), with predicted values in the range of 90% confidence interval performed using the built-in population simulator in GastroPlus™. Model-predicted C_{max}, AUC_{0-t}, V_d, and systemic clearance (CL_{sys}) met the verification criterion, with predicted/observed ratio in the range of 0.80–1.2 and are presented in Table 4.
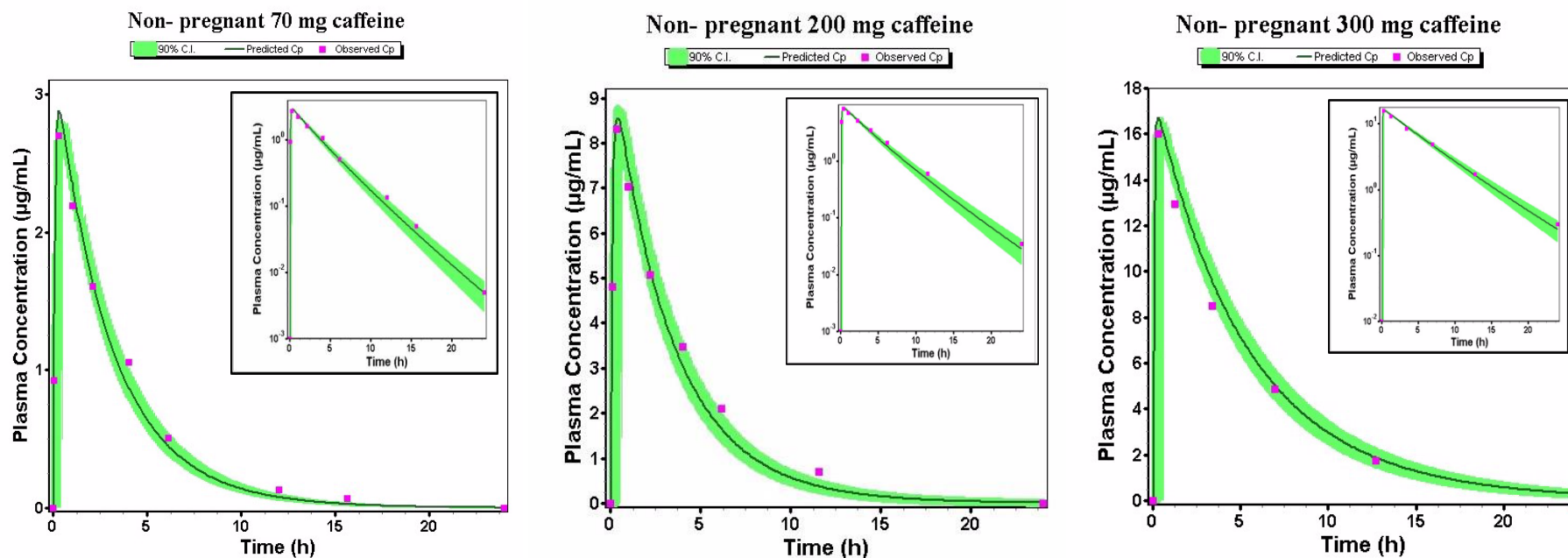
Figure 2. Predicted and observed plasma concentration-time profiles of caffeine after administration of single oral doses at 70, 200 and 300 mg to non-pregnant women. The square symbols represent the mean of observed data, and solid lines represent the predicted mean of caffeine profiles. Inserts contain caffeine plasma profiles in semi-log scale. Green shaded areas represent the 90% confidence interval for the simulated data.

Table 4. Predicted and observed pharmacokinetic parameters in non-pregnant and pregnant populations after single doses of caffeine at 70, 200 and 300 mg.

Caffeine dose		Parameter	C_{max} (µg/ml)	T_{max} (h)	AUC_{0-t} (µg.h/ml)	V_d (l/kg)	Cl_{sys} (l/h)	$t_{1/2}$ (h)
70 mg	Non-pregnant	Observed	2.5	0.2	9.5	0.51	6.3	4.5
		Predicted	2.7	0.3	9.8	0.60	5.0	7.6
		Pred/Obs	*1.08*	*1.5*	*1.03*	*1.17*	*0.80*	*1.68*
	T1	Predicted	3.7	0.4	14.1	0.65	4.9	8.0
	T2	Predicted	3.8	0.4	16.2	0.70	4.3	8.1
	T3	Observed	4.1	0.5	-	-	-	-
		Predicted	3.9	0.4	26.9	0.70	4.3	10.8
		Pred/Obs	*0.95*	*0.8*				
200 mg	Non-pregnant	Observed	8.5	0.3	31.6	0.54	4.8	6.0
		Predicted	8.5	0.4	32.4	0.60	4.9	9.0
		Pred/Obs	*1.0*	*1.33*	*1.03*	*1.11*	*1.02*	*1.5*
	T1	Predicted	8.6	0.4	44.1	0.65	4.5	9.8
	T2	Predicted	8.6	0.5	45.6	0.70	4.3	11.0
	T3	Observed	8.4	0.5	-	-	-	-
		Predicted	8.8	0.5	74.3	0.72	4.1	15.0
		Pred/Obs	*1.05*	*1.0*				
300 mg	Non-pregnant	Observed	16.5	0.2	91.9	0.55	4.5	6.4
		Predicted	16	0.2	91.3	0.60	3.2	13.0
		Pred/Obs	*0.97*	*1.0*	*0.99*	*1.09*	*0.71*	*2.03*
	T1	Predicted	16.3	0.4	91.5	0.72	3.5	13.1
	T2	Predicted	16.6	0.5	152.8	0.72	3.2	15.0
	T3	Predicted	16.9	0.5	170.3	0.75	3.1	18.0

Non-pregnant observed values from reference (Cheng *et al.*, 1990).

Pregnant observed values from reference (Kirkinen *et al.*, 1983*a*, *b*).

- Not available
- Pred/Obs: Predicted/Observed

Development and Verification of PBPK Model in Pregnant Subjects

Concentration-time profiles from pregnant women in third trimester were used to construct and validate the PK model (Braizer JL, 1983). The model was developed and validated against the disposition kinetics of caffeine after administration of 150 mg single dose (Braizer JL, 1983). As shown in Figure 3, the simulated plasma concentrations-time profile captured the observed PK parameters with predicted values in the range of 90% confidence interval. The validated PBPK model was then used to develop a PBPK model for virtual pregnant population (p-PBPK) over the three trimesters, which takes into account the physiological changes during pregnancy and the FPC (Figure 1, Table 3), in addition to changes in maternal CYP1A2 activity. Concentration-time profiles were built and PK parameters were predicted for the three caffeine doses of 70, 200 and 300 mg used for the non-pregnant model. The model was able to predict observed T_{max} (between 0.4-0.5 h) and C_{max} values for 70 (4.1 vs 3.9 µg/ml) and 200 mg (8.4 vs 8.8 µg/ml) for T3 of pregnancy (Kirkinen *et al.*, 1983*a*). In addition, and as expected, caffeine exposure was significantly increased as a function of dose across the trimesters, which is consistent with previous studies reported a significant prolongation of caffeine elimination half-life in pregnant women (Braizer JL, 1983; Gaohua *et al.*, 2012).

The effect of CYP1A2 downregulation in pregnancy was obvious on the decreased Cl_{sys} and increased $t_{1/2}$ as a function of dose (Table 4). The model predicted a prolonged $t_{1/2}$ from 7.6 h in non-pregnant to 10.8 h in 70 mg dose, 15 h in 200 mg dose, and 18 h in 300 mg dose in the third trimester of pregnancy. Reduced clearance and increased $t_{1/2}$ were associated with a significant increase in AUC values as presented in Table 4. Other changes in caffeine PK parameter across the 3 trimesters are presented in Table 4. Compared to non-pregnant subjects, a gradual significant increase in V_d was also predicted as pregnancy progresses.
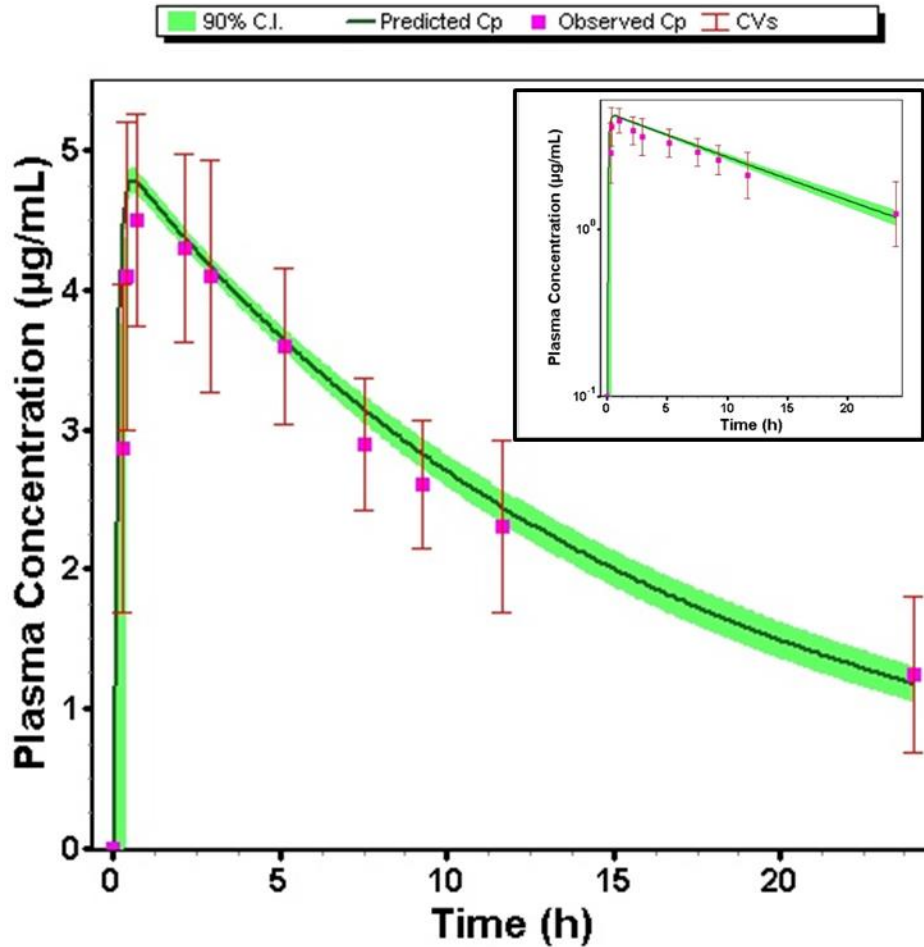
Figure 3. Predicted and observed plasma concentration-time profiles of caffeine in pregnant women in their third trimester following the administration of a single 150 mg oral dose. The square symbols represent the mean of observed data, and solid lines represent the predicted mean of caffeine profiles. Inserts contain caffeine plasma profiles in semi-log scale. Green shaded areas represent the 90% confidence interval for the simulated data. Observed data was obtained from (Braizer JL, 1983).

Maternal PK parameters and profile were used to predict caffeine concentration in the FPC in the three trimesters. Based on predicted concentration-time profiles in pregnant women, caffeine concentration-time profiles in T1, T2 and T3 in the FPC of the three evaluated doses were also predicted (Figure 4). The model predicted a significant increase in caffeine concentration in the FPC with prolonged half-life, which increased across the trimesters as a function of dose.

Caffeine Multiple Dosing Data Validation

Non-pregnant and pregnant women could consume caffeine multiple times a day as well, so an assumption was made that an ingestion of three times daily of caffeine from different resources was acceptable. Thus, the model was further validated by using steady state concentrations from the literature (Birkett and Miners, 1991). In this study, caffeine was used at 150 mg dose administered three times daily in non-pregnant subjects (Birkett and Miners, 1991). Pharmacokinetic parameters from (Birkett and Miners, 1991) were used to validate the predicted data from GastroPlus such as C_{maxSS}, Cl_{sys} and Cl_R, which were then used to predict parameters at 300 mg multiple dosing in non-pregnant subjects, pregnant women and changes across the 3 trimesters. The results are listed in Table 5. For the 150 mg dose, predicted values for C_{maxSS}, Cl_{sys} and Cl_R were consistent with the observed values in non-pregnant subjects with predicted/observed in the range of 0.80–1.2 (Table 5). At both doses, predicted values across the 3 trimesters revealed that while renal clearance remained the same, the systemic clearance and hence C_{maxSS} gradually decreased and increased, respectively, because of reduced CYP1A2 activity caused by pregnancy. Comparing the 300 mg dose in pregnancy, C_{maxSS} and AUC were higher than single dosing at T3 by ~1.4- and 2.9-fold, respectively, due to the steady state effect.

53
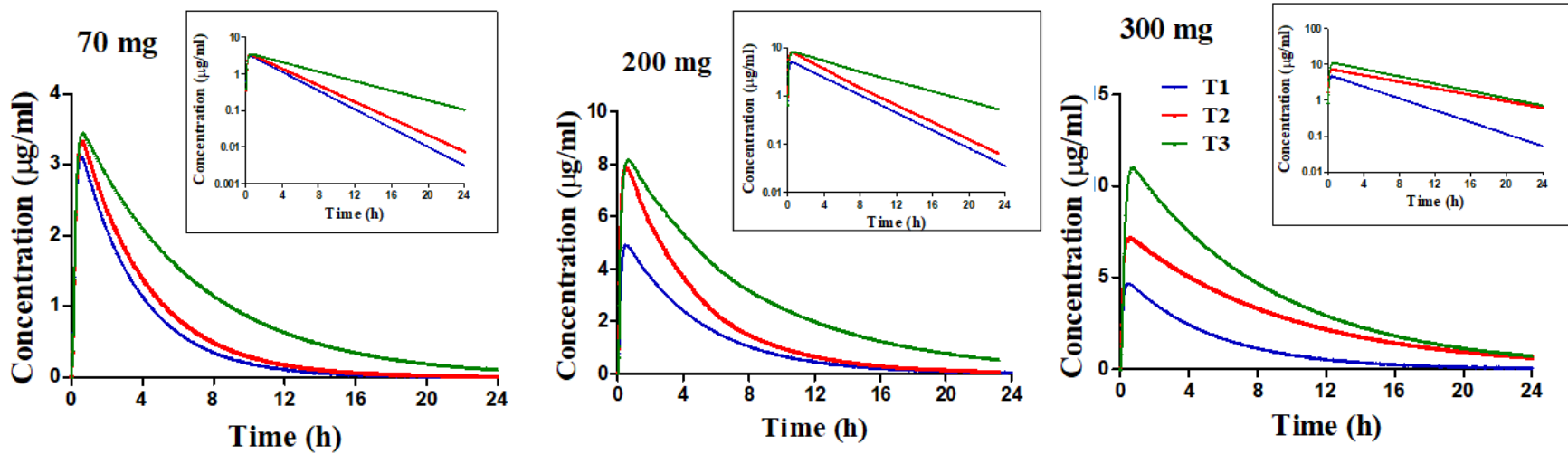
Figure 4. Predicted caffeine concentrations-time profiles in the fetoplacental compartment (FPC) over the three trimesters (T1, T2 and T3) following the administration of single oral doses of caffeine at 70, 200 and 300 mg. Inserts contain caffeine FPC concentration-time profiles in semi-log scale.

Table 5. Predicted vs. observed steady state pharmacokinetic parameters of caffeine at 150 and 300 mg administered three times daily in non-pregnant and pregnant subjects (Birkett and Miners, 1991).

Pregnant subjects

| Caffeine dose | C_{maxSS} (µg/ml) | | AUC_{0-t} (µg.h/ml) | Cl_{sys} (l/h) | | Cl_R (l/h) | |
	Observed	Predicted	Predicted	Observed	Predicted	Observed	Predicted
150 mg Q8[*]	6.7	7.1	62.4	4.5	4.7	0.032	0.038
Non-pregnant	*Pred/Obs*	*1.06*		*Pred/Obs*	*1.05*	*Pred/Obs*	*1.19*
T1	-	7.8	99.8	-	4.5	-	0.038
T2	-	8.0	110.0	-	4.2	-	0.038
T3	-	11.1	178.9	-	4.0	-	0.038
300 mg Q8[*]							
Non-pregnant	-	16.1	199.7	-	4.8	-	0.032
T1	-	16.9	277.4	-	3.6	-	0.032
T2	-	17.5	371.7	-	3.3	-	0.032
T3	-	22.3	498.8	-	3.0	-	0.032

C_{maxSS} is C_{max} at steady state; *Q8; three times per day; - not available; observed values from (Birkett and Miners, 1991).

Pharmacodynamics Models

It has been reported that PDE inhibition is inversely related to cAMP levels, which are correlated with maternal caffeine concentrations (Paul Weathersbee, 1977, Kirkinen *et al.*, 1983*b*; Montaya, 2005). To monitor the effect of caffeine in pregnancy, the developed models were fitted for the reported PD responses after caffeine administration based on caffeine concentration-time profiles (Montaya, 2005). In the non-pregnant model, reported PD responses on the 7th day C_{max} for 179 and 618 mg caffeine doses administered once daily for one week were used to validate the model. At both doses, the indirect model successfully predicted caffeine effect on PDE in non-pregnant subjects (Table 6) (Montaya, 2005). Similarly, for cAMP, the direct PD model at the high dose (618 mg) demonstrated close match between observed and simulated PD effect of caffeine (Table 6). When predicted for pregnancy, increasing the dose from 70, 200 to 300 mg demonstrated a gradual decrease in PDE activity and increase in cAMP levels predicted at caffeine C_{max} across the trimesters as shown in Figure 5, which demonstrates a correlation between C_{max}, PDE and cAMP where increased C_{max} as a function of dose and trimester is associated with decreased PDE and increased cAMP.

In addition, a direct PD model for epinephrine was developed. Average normal epinephrine levels in non-pregnant subjects is around 25 ng/l, and epinephrine levels usually increase with caffeine intake (Kirkinen *et al.*, 1983*a, b*), which was successfully predicted by the developed model where epinephrine level at C_{max} increased from 31.7 to 40.3 ng/l at 179 and 618 mg doses, respectively (Table 6). To validate the model in pregnancy, caffeine at both 70 and 200 mg administered as single doses in the third trimester were compared to a reported observed C_{max} data (89.5 and 124.7, respectively (Kirkinen *et al.*, 1983*a, b*), and the results showed our model successfully predicated epinephrine at both doses (Table 6). Next, the model was used to predict epinephrine levels for first and second trimesters, and for 300 mg caffeine; the results

56

demonstrated that following a single caffeine dose, epinephrine blood levels increases with

increased caffeine dose and across the trimesters (Table 6).

Figure 5. Predicted caffeine Cmax in non-pregnant and pregnant women at three different single doses (70, 200 and 300 mg) for the three trimesters of pregnancy, and its correlation to predicted PDE and cAMP levels. Each category represents a caffeine dose; First grey: 70 mg, White: 200mg, second grey: 300mg caffeine. Non is for non-pregnant.
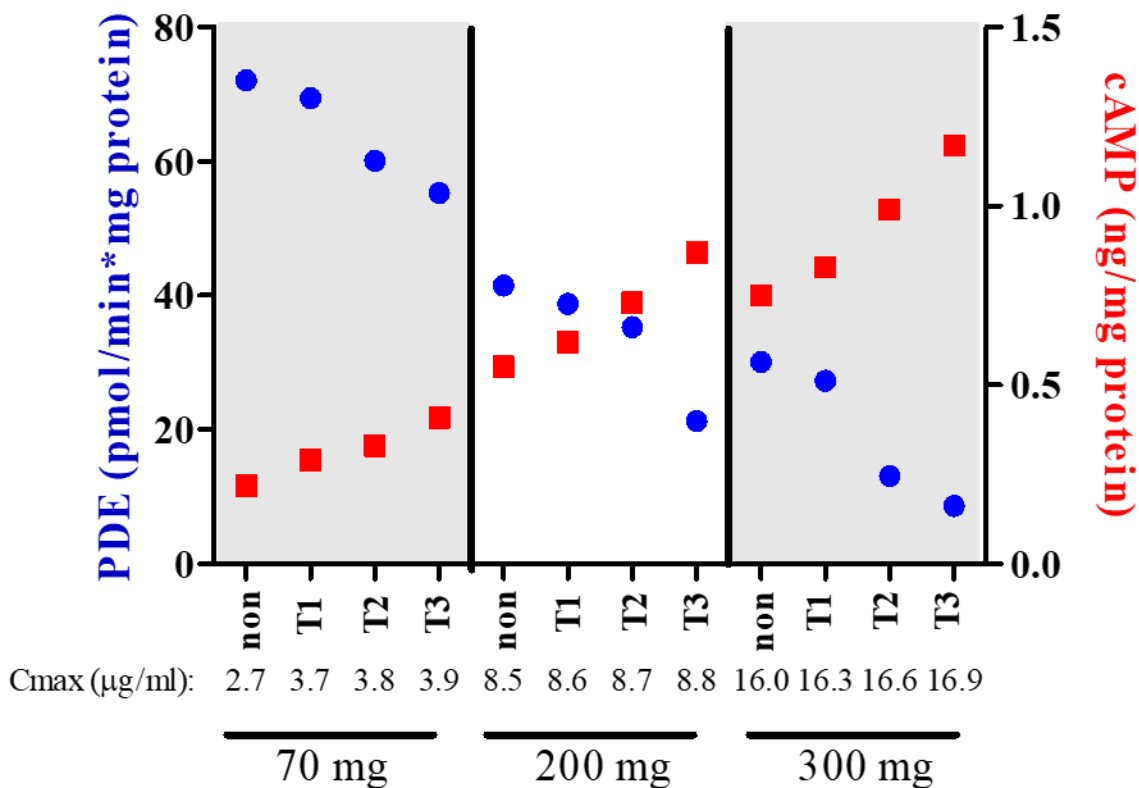
Table 6. Observed and predicted values of PDE, cAMP and epinephrine at observed caffeine C_{max} values following its daily dosing for one week at 179 and 618 mg in non- pregnant, and predicted values following a single dose at 70, 200 and 300 mg in pregnant subjects.

Non-pregnant subjects (All observed data were from Reference (Montaya, 2005))

Caffeine dose	C_{max} Predicted (μg/ml)	PDE[#]		cAMP[*]		Epinephrine[!]	
		Observed	Predicted	Observed	Predicted	Observed	Predicted
179 mg	8.5	72.5	72.3	-	-	-	31.7
618 mg	32.3	5.5	7.1	0.9	0.91	-	40.3

Pregnant subjects (All observed data were from Reference (Kirkinen *et al.*, 1983*a*, *b*)

Caffeine dose	Parameters				
	C_{max} Predicted (µg/ml)	PDE[#] Predicted	cAMP[*] Predicted	Epinephrine[!] Observed	Predicted
70 mg					
Non-pregnant	2.7	72.1	0.22	-	27.1
T1	3.7	69.4	0.29	-	53.3
T2	3.8	60.1	0.33	-	61.3
T3	3.9	55.3	0.41	89.5	71.5
200 mg					
Non-pregnant	8.5	41.5	0.55	-	32.1
T1	8.6	38.8	0.62	-	70.2
T2	8.7	35.3	0.73	-	91.6
T3	8.8	21.3	0.87	124.7	121.5
300 mg					
Non-pregnant	16.0	30.1	0.75	-	36.2
T1	16.3	27.3	0.83	-	83.1
T2	16.6	13.1	0.99	-	106.3
T3	16.9	8.6	1.17	-	145.7

pmol/min*mg protein; * ng/mg protein; ! ng/l; - not available.

Discussion

Several physiological and biological changes occur during pregnancy that can affect drugs disposition, however, it is impossible to study changes in PK of all drugs administered during pregnancy. Hence, PBPK models are developed to validate and predict drugs disposition and effect on the body using a physiologically realistic compartmental structure with sets of differential equations. This method has the benefit of incorporating both physiological parameters that change in pregnancy (e.g., time-varying changes in maternal weight, individual organ volumes/blood flows, cardiac output, glomerular filtration rate, and drug-metabolizing enzyme activities) that are important for ADME processes, and drug-specific parameters (e.g., physicochemical and in vitro metabolism/transport characteristics) (Montoya *et al.*, 2014).

Several studies have reported caffeine disposition in pregnancy in real and virtual populations (Weng, X.; 2008, Gaohua, L.; 2012, Kirkinen *et al.*, 1983*a*, *b*); 1983, Xia, B.; 2013, Ke *et al.*, 2018*a*), Dallmann, A.; 2018). In addition, several reports related the risk of miscarriage with caffeine intake >200 mg per day, Okubo, H.; 2015, COT Statement 2001/06,2001, WHO , 2016, EFSA, 2015). Thus, in the current study, we verified and extended previously developed PBPK models for caffeine in pregnant population to predict changes on caffeine PD parameters associated with miscarriage risk namely PDE, cAMP and epinephrine (Monatay,; 2005, (Kirkinen *et al.*, 1983*a*, *b*), Weathersbee, P. S.;1977).   The developed pregnancy PBPK/PD model that considered caffeine physiochemical and PK parameters, and physiologic and metabolic changes that occur normally during pregnancy successfully predicted changes in maternal caffeine plasma levels and PD-related parameter at different stages of pregnancy. In addition, the pregnant PBPK model predicted the increase in caffeine accumulation in the fetoplacental compartment over the trimesters.

Consistent with other developed PBPK models based on Simcyp and PK-sim for caffeine in non-pregnant and pregnant women, our developed PBPK model using Gastroplus successfully simulated and predicted caffeine plasma concentration-time profiles and PK parameters following single and multiple dosing. In non-pregnant population, simulated caffeine PK parameters exhibited non-linear kinetics, which is consistent with the reported observed data (Cheng *et al.*, 1990) For example, C_{max} increased from 2.5, 8.5 to 16.5 µg/ml at caffeine doses of 70, 200 and 300 mg, respectively; similar behavior was observed with the parameters AUC, Cl_{Sys} and $t_{1/2}$ indicating saturable caffeine metabolism by CYP1A2 in the dose range tested. The model predictive performance was reliable as evaluated by predicted C_{max}, AUC, V_d, and Cl_{sys} with values being within ±20% of the observed data for the 3 doses with the exception for Cl_{sys} at 300 mg dose (predicted/observed data is 0.71) and $t_{1/2}$ at the 3 doses (predicted/observed data ranged from 1.5-2.03; Table 4). This is acceptable due to reported caffeine variable half-life in non-pregnant subjects ranging from 1.5 to 10 hours that increases with increasing the dose (Cheng *et al.*, 1990).

Next, we developed and verified the pregnant PBPK model. This model accounted for CYP1A2 down regulation in each trimester in addition to other known pregnancy-induced changes presented in Table 3. As expected, the effect of reduced CYP1A2 activity by pregnancy and across the three trimesters exhibited non-linear kinetics and significantly increased caffeine exposure (AUC) by 2- to 3-fold, decreased systemic clearance and prolonged $t_{1/2}$, a pattern that is consistent with previously reported findings (Gaohua, L.; 2015, Kirkinen *et al.*, 1983*a*, *b*), Partosch, F.; 2015, Dallmann, A.; 2018). Also, an increase in V_d was observed, mainly in the third trimester, which could be due to water-weight gain in pregnant woman; caffeine is a water soluble compound and prefers to distribute to the new water-gained weight area, which increases

the V_d. Besides, the pregnant-PBPK model predicted caffeine concentration-time profile in the

FPC. As demonstrated in Figure 4, caffeine accumulated in the FPC with prolonged half-life as a

function of dose across the three trimesters. For example, with the 300 mg caffeine dose,

predicted $t_{1/2}$ increased from 5 to 8 h in the third trimester. This behavior is expected as caffeine

exposure in the FPC parallels that of the maternal blood. On the other hand, based on Kirkinen

and colleagues study (Kirkinen *et al.*, 1983*a*, *b*), a 200 mg caffeine dose reduced intervillous

blood flow by 25% in T3 of pregnancy, a parameter that was included in the pregnancy model.

This reduction in intervillous blood flow caused a 12.5% reduction in diffused amount of

caffeine to the fetus across the placenta, and thus lower FPC-caffeine exposure than what would

be expected if caffeine didn't alter the intervillous blood flow by 25%. While the effect of

caffeine at lower and higher doses than 200 mg on the intervillous blood flow is unknown, we

assumed similar 25% reduction in intervillous blood flow for T1 and T2 of pregnancy and with

other tested caffeine doses (i.e. 70 and 300 mg).

Following PBPK models validation, a PD model was developed to evaluate the effect of

increased plasma levels of caffeine on PDE, cAMP and epinephrine, parameters associated with

miscarriage risk study (Kirkinen *et al.*, 1983*a*, *b*, Li, J.;2015). While pregnancy could induce

changes in the evaluated PD parameters, in the model, we assumed PD in non-pregnant and

pregnant women are the same. Yet, the model successfully predicted epinephrine levels in third

trimester that was comparable with reported observed values (Table 6) (Kirkinen *et al.*, 1983*a*, *b*)

(Kirkinen, P.;1983 is this 1983a or 1983b?, Montoya, et al 2014). To predict effect of caffeine on

these parameters in pregnancy, PDE activity and cAMP concentrations were validated for high

(618 mg) and low (179 mg) single doses of caffeine that were compared to non-pregnant subjects

as presented in Table 6. The model successfully predicted changes in PD parameters as a

function of dose in non-pregnant subjects, and concluded a significant decrease in PDE and increase in cAMP levels at higher doses of caffeine (Table 6, Figure 5). Similarly, the p-PKPD model successfully predicted the effect of different doses of caffeine on PDE, cAMP and epinephrine levels in pregnant women. Compared to normal epinephrine levels of 25 ng/l (Doepker, C.;2018), predicted data for the 3 trimesters revealed increased levels of maternal epinephrine. In the third trimester, observed data following 70 and 200 mg doses of caffeine showed increased epinephrine levels by 3 to 5- fold compared to non-pregnant levels, and the predicted data for both doses was consistent with observed levels (Kirkinen *et al.*, 1983*a*, *b*). For 300 mg dose, epinephrine increased approximately by 5-fold. Such high levels of epinephrine could cause a significant decrease in intervillous blood flow, which could increase the risk of pregnancy loss (Kirkinen *et al.*, 1983*a*, *b*). The limitation of the study it did not consider higher doses of caffeine as it was hard to verify the model for higher doses due to lacking literature data.

Conclusions

PBPK modeling and simulation has been used recently to predict drugs action to support or as an alternative for clinical investigations especially in patient populations where clinical trials are not possible. This study highlights the utility of PBPK/PD modeling and the unique application of the PBPK model to a PD outcome that could be utilized to help define potential cut-offs for caffeine intake in various stages of pregnancy. Our work verified that caffeine maternal blood levels increase with pregnancy due to progressive reduction in its metabolism by CYP1A2. CYP1A2 is downregulated as pregnancy progresses. Caffeine increase leads to reduced levels of PDE, increased levels of cAMP and epinephrine. For example, in the third

trimester, daily intake of 200 mg or more of caffeine increased epinephrine blood levels by 4-fold and higher when compared to normal levels, which could increase risk of pregnancy loss. Epinephrine is a vasoconstrictor, at high levels it could reduce the blood flow to the placenta causing complications. Therefore, pregnant women are advised to limit their caffeine intake. While further clinical investigations are necessary, our findings could assist in designing clinical investigations to understand caffeine-miscarriage association better and thus prevent such risk.

Chapter 3

Modeling and simulation of the effect of P-glycoprotein and lysosomal entrapment, and genetic variation in metabolizing enzymes on granisetron PK and PD

Abstract

Chemotherapy-induced nausea and vomiting (CINV) is one of the most undesirable side effects that affect a patient's quality of life. Granisetron is one of the most widely used 5-hydroxytryptamine 3 (5-HT3) receptor antagonists in the field of CINV. Granisetron is effective in many cases; however, about 20-30% of patients remain to show unsatisfactory responses. The purpose of this work is to explain the variability in granisetron efficacy. First, we identified the role of P-gp and lysosomal entrapment on granisetron intestinal permeability and plasma profiles following oral dosing using the transport study. In this study, we showed that granisetron as a P-gp substrate and based on its physiochemical properties susceptible for lysosomal entrapment, and thus limiting permeability across Caco2 cell monolayer *in-vitro*. Also, we investigated and predicted the effect of P-gp and lysosomal modulation and interplay on granisetron levels using MembranePlus software. We were able to predict the effect of P-gp and lysosomal entrapment on granisetron permeability, where P-gp inhibition and increasing lysosomal pH would increase granisetron permeability.

As another cause of variability, we evaluated the effect of genetic polymorphism in CYP1A1 and CYP3A5 on granisetron PK and PD. For this, we developed a PKPD model to validate and predict the effect of genetic variations in CYP1A1 and CYP3A5 on granisetron levels in plasma and brain and predict the impact of these genetic variations on the occupancy of 5-HT3 receptors where lower occupancy was noticed with the CYP1A1 *2A SNP as an extensive metabolizer, and higher occupancy with the CYP3A5 *3 SNP as a poor metabolizer.

Introduction

Chemotherapy-induced nausea and vomiting (CINV) is one of the most undesirable side effects that affect a patient's quality of life. Serotonin, released from the enterochromaffin cells of the small intestine after the administration of chemotherapeutic agents, activates both peripheral and central 5-hydroxytryptamine 3 (5-HT3) receptors on vagal nerve terminals and central structures (Navari, 2009, 2015; Smith *et al.*, 2019). 5-HT3 receptor antagonists are one of the most effective antiemetic agents for suppressing acute phase CINV prophylaxis (Kilpatrick, 1990; Engel *et al.*, 2013). 5-HT3 receptor antagonists suppress CINV by preventing serotonin binding to 5-HT3 receptors (Engel *et al.*, 2013). 5-HT3 receptors are distributed in many brain regions, with the highest levels of distribution in the brainstem, especially in regions involved in vomiting reflex such as the area postrema (AP); 5-HT3 receptors binding sites in the CNS was first recognized using a radiolabeled 5-HT3 receptor antagonist namely [3H]GR65630 (Kilpatrick *et al.*, 1987; Tecott *et al.*, 1993; Miller and Leslie, 1994; Aapro *et al.*, 2015; Zhang *et al.*, 2016).

Granisetron is one of the most widely used 5-HT3 receptor antagonist drug in the field of CINV. Granisetron is effective in many cases, however about 20-30% of patients remain to show unsatisfactory responses (Kioka *et al.*, 1989; Darmani, 1998; Zhong *et al.*, 2014). P-glycoprotein (P-gp), is a member of the adenosine triphosphate (ATP)-binding cassette family and is encoded by human ABCB1 gene (ATP-binding cassette, subfamily B), also called MDR1 (multidrug resistance protein) (Hodges, 2011; Tsuji *et al.*, 2017). P-gp functions as a transmembrane efflux pump that transports various molecules out of the cell; it works by identifying substrates and moving them out of the cell (from intracellular to extracellular). It also identifies substrates trapped in the cell membrane and efflux them out of the cells (Fromm and Kim, 2011; Hodges,

2011; Meszaros *et al.*, 2013). P-gp is found in the canalicular surface of hepatocytes, the apical

surface of proximal tubular cells in kidneys, and the brush border surface of enterocytes (Fromm

and Kim, 2011). In addition, P-gp is expressed in the epithelium of the brain choroid plexus

(which forms the blood–cerebrospinal fluid barrier), as well as on the luminal surface of blood

capillaries of the brain namely on the endothelial cells of the blood-brain barrier (Hodges, 2011).

To be a substrate, the drug has to be lipophilic, and the number of hydrogen bonds appears to be

a relevant parameter, as both have been proportionally correlated to the affinity of compounds

for P-gp. Whether granisetron is a P-gp substrate or not requires further evaluation (Von Richter

et al., 2009); however, available reports on other 5-HT3 receptor antagonists drugs have

demonstrated ondansetron as a substrate for P-gp (Durieux, 1995). Lysosomes are acidic

organelles (pH 4–5), its main function is in degrading macromolecules, the turnover of

phospholipids, breakdown of endogenous waste products, autophagy, and apoptosis (Daniel and

Wójcikowski, 1997). It was first studied by de Duve et al. in (1974), where they described the

function of lysosomes in sequestering or entrapping drugs through a non-enzymatic, non–

transporter-mediated process known as lysosomal trapping. To get entrapped inside a lysosome,

a drug should exhibit a lipophilic feature (LogP > 1), and amphiphilic drugs with ionizable

amines (pKa > 6) can also accumulate in lysosomes (Kazmi *et al.*, 2013; Zhitomirsky and

Assaraf, 2015, 2017). A greater proportion of the total concentration of these drugs are present as

a non- protonated neutral molecule at physiologic pH (7.2–7.4) and can readily pass across cell

membranes by passive diffusion (Kazmi *et al.*, 2013; Zhitomirsky and Assaraf, 2015). Inside the

lysosomes, an equilibrium shift towards the protonated form occurs because of the lysosomal

acidic environment (pH 4–5), which restricts the movement of the drug back through the

lysosomal membrane into the cytosolic space (Zhitomirsky and Assaraf, 2015). Compared with

the blood pH (7.4), the cytosolic pH is a bit more acidic (7.0–7.2), and that could play a significant role in drug disposition such as granisetron, which becomes highly sequestered in lysosomes (Zhitomirsky and Assaraf, 2015).

About 20-30% of patients receiving granisetron for the prevention of CINV still suffer from nausea and vomiting (Kioka *et al.*, 1989; Darmani, 1998; Zhong *et al.*, 2014). While several factors could play a role in the variation of granisetron efficacy, in this work, we will evaluate the effect of modulating P-gp and lysosomes on granisetron permeability and plasma levels following oral administration. The second part of the study will predict the effect of genetic variations in CYP enzymes on granisetron plasma and brain levels, and ultimately receptor occupancy. Granisetron is mainly cleared by hepatic metabolism, with less than 20% of the dose is eliminated unchanged in urine. Granisetron is metabolized primarily by cytochrome P450 1A1 (CYP 1A1) and CYP 3A5, as established by ketoconazole inhibition studies in *in-vitro* liver microsomal studies (Nakamura *et al.*, 2005; Bustos *et al.*, 2016). Thus, the purpose of this work is to first, develop a mechanistic model for *in-vitro* analysis of granisetron permeability, considering P-gp efflux and lysosomal entrapment, which was then validated by analyzing the effect of inhibitors on its apparent permeability using MembranePlus™ and plasma profile following oral administration using GastroPlus^{TM}. Second, to develop a PKPD model to validate and predict the effect of genetic variations in CYP1A1 and CYP3A5 on granisetron levels in plasma and brain and predict the effect of these genetic variations on the occupancy of 5-HT3 receptors by granisetron using GastroPlus^{TM}.

Materials and methods

Materials

Granisetron hydrochloride was purchased from Tokyo chemicals industry, Co., LTD (Portland, OR). Ammonium chloride was purchased from Macron fine chemicals (Radnor, PA), and verapamil hydrochloride and triethyllamine (TEA) were obtained from Sigma Aldrich (MO, USA). Bafilomycin A1 was obtained from Alfa Aesar (Tewksbury, MA). Acetonitrile and methanol, HPLC grade, were obtained from EMD Chemicals (Burlington, MA). Dulbecco's modified Eagle medium (DMEM), fetal bovine serum (FBS) and penicillin–streptomycin (10000 I.U.-10 mg/ml) were obtained from American Type Cell Culture Collection (ATCC; Manassas, VA). Deionized water (DI) was used for all preparations.

Cell culture and *in-vitro* assay for granisetron transport across Caco2 cells monolayer

Caco2 cells (passage numbers 40-60) were cultivated in DMEM media supplemented with 20% FBS and 2.5% antibiotics in a humidified incubator with 5% CO2 at 37 °C. The cells were cultured on a 75 cm² flask at a density of 1×10^6 cells/flask and were then harvested at 90% confluence with trypsin–EDTA. For the preparation of Caco2 cell monolayers, cells were plated in a 12-well transwell plate (1.131 cm^2 membrane surface area, 13.85 mm diameter; Corning Inc., Tewksbury, MA). The culture medium was renewed every other day with 0.5 ml and 1.5 ml into the apical and basolateral sides, respectively.

In-vitro transcellular transport of granisetron was performed to determine P-gp-mediated transport parameters in both directions, apical to basolateral (A➔B) and basolateral to apical

(B→A). Transport experiments were performed in triplicates, as described below. Caco2 cell monolayer was pre-incubated in HEPES buffer for 30 min at 37 °C. Then, the transepithelial electrical resistance (TEER) was estimated with the Millicell-ERS system (Millipore Co., Bedford, MA) to confirm monolayer formation. Caco2 monolayers with TEER values over 300 Ωcm^2 were included in the experiments. To begin the experiment, granisetron was diluted in transport buffer to make different concentrations ranging from 10 to 400 µM and added to apical or basolateral sides of the insert. To determine the passive permeability of granisetron, verapamil, as a P-gp inhibitor, was co-incubated at a concentration of 100 µM in the apical side(Durie and Dalton, 1988). To determine lysosomal entrapment of granisetron, ammonium chloride (NH4Cl) was added at a concentration of 20 mM in the apical side (Ufuk *et al.*, 2015). Samples were taken from the apical and the basolateral side (100 µl) at 0, 0.5,1, 2, and 4 hours and replaced with transport buffer. Concentrations of granisetron in the samples were measured by high-performance liquid chromatography (HPLC), as described below. P-gp Vmax and Km, efflux ratios, and lysosomal entrapment were calculated from the *in-vitro* studies. These values were used and optimized as input parameters in MembranePlus and GastroPlus to predict the effect of P-gp and lysosomal entrapment on granisetron permeability.

Measurement of cell viability assay using MTT

3-(4,5-Dimethylthiazol-2-yl)-2,5-diphenyltetrazolium bromide (MTT) was used to measure cell viability. The MTT based cell viability was determined based on published reports by Zheng et al., 2014. Caco2 cell lines were incubated with different concentrations of granisetron in the range (10-400µM) for 24 h. MTT 1mg/ml was added for 4 h at 37°C and the dark blue formazan

crystals formed were dissolved in DMSO and was subjected to colorimetric measurement at 570 nm using a microtiter plate reader.

Western Blot Analysis to Confirm P-gp Expression

Twenty-five micrograms of protein samples were applied and resolved using 10% SDS−polyacrylamide gel at 140 V for 1.5 h and transferred electrophoretically to PVDF membrane at 300 mA for 2 h at 4 °C. PBS solution containing 3% BSA was used to block nonspecific binding while rocking at room temperature for 1 h. Membranes were then incubated with primary antibodies overnight at 4 °C. Primary antibodies used for P-gp (C-219) and β-actin. Secondary antibodies used were HRP- conjugated anti-mouse IgG secondary antibodies (1:1000) dilutions for P-gp and β-actin. Blots were formed using a chemiluminescence detection kit (ThermoFisher). Bands were pictured using ChemiDoc MP Imaging System (Bio-Rad Hercules, USA). Image Lab Software V.6.0 (Bio-Rad) was used to quantify the resultant bands.

HPLC analysis of granisetron

HPLC analysis was achieved by an isocratic Prominence Shimadzu HPLC system (Columbia, MD). The system consisted of a SIL 20-AHTautosampler, fluorescence detector (Shimadzu, RF10A XL), PDA detector and a LC-20AB pump connected to a Dgu-20A3 degasser. Data acquisition was achieved by LC Solution software version 1.22 SP1.
The chromatographic conditions consisted of a Luna 5 μm C18 column (250 × 4.6 mm i.d.; Phenomenex, USA); the mobile phase was a mixture of phosphate buffer (5 mM, pH 3.0), methanol and acetonitrile (25:40:35 v/v/v) containing 1% triethylamine (TEA), delivered at 1.0 ml/min flow rate. Standard curves of granisetron were prepared in the range of 0.5 to 50 μM.

Validation of the developed HPLC method

System parameters were evaluated by using a solution of granisetron (100 µg/ml in mobile phase). Six replicates were injected to the HPLC system. The linearity of the method was evaluated by constructing six series of calibration curves using granisetron solutions of 0.5, 1, 5, 10 and 50 µg/ml prepared by subsequent dilution of stock standard solution of granisetron in acetonitrile. The inter-day and intra-day accuracy and precision was established by using three replicates of standard solutions of granisetron at three different concentrations (0.5, 5 and 50 µg/ml) during a single day and three separate days. The stability of granisetron standard solutions (10 µg/ml in acetonitrile) was checked after storing at room temperature for 1 week. The concentration of granisetron samples was determined and compared with freshly prepared samples. Lower limit of detection (LOD) and lower limited of quantification (LOQ) were calculated: LOD by measuring three replicates of spiked sample, taking the AUC of the peak at the same retention time of granisetron and compare it to the AUC of the same retention time in a blank sample to get a signal/noise ratio of 3. LOQ is the lowest concentration in the calibration curve that give reliable levels with CV <20%.

Development of a PBPK model for granisetron

All PBPK simulations were carried out using MembranePlus™ and GastroPlus™ integrated with ADMET Predictor (Simulation Plus Inc., Lancaster, CA). MembranePlus™ is a software platform for simulation of passive and active drug transport in various cell assays. MembranePlus give us the opportunity to simulate and predict drug concentrations based on *in-vitro* based assays, where we are able to calculate permeability and other parameters for *in-vivo* extrapolation, by integrating multiple experimental and cellular processes, for example, lysosomal trapping parameters, carrier-mediated transport and protein binding (Szeto *et al.*,

2007). Input parameters are presented in Table 7-1. In this work, MembranePlus™ was used to

assess, validate, and predict the transport of granisetron through Caco2 cells from the data

acquired from *in-vitro* experiments. P-gp Vmax and Km calculated from the *in-vitro* experiments

(P-gp Vmax 0.029 µM/sec and P-gp Km 43.93 µM) were used as input data where they were

optimized by the software (P-gp Vmax 0.035 µM/sec and P-gp Km 49.1 µM) for better

prediction of the amount transported across the monolayer. MembranePlus™ was also used to

predict the effect of changes in lysosomal pH (from 6 to 4) on the entrapment of granisetron

inside the lysosomes, where data from *in-vitro* experiments using bafilomycin A1 were used as

input parameters. Table 7-2 shows the differences in physiochemical values between ADMET

prediction and literature reports. It was noted when comparing the values from ADMET and

from different literature resources that granisetron molecular weight, solubility, LogP and pKa

are comparable or close values to those predicted by ADMET, thus we don't expect an effect on

the modeling when these small changes are applied.

Table 7-1. The input parameters that are used in both MembranePlus and GastroPlus.

Input Parameter	Value	Reference
Molecular weight (g/mol)	312.41	A
Solubility (mg/ml) pH=7	17	A
LogP	2.2	A
Diffusion coefficient (cm²/sec)	0.722×10^{-5}	A
Inonization constant (Pka)	9.21 (base)	A
Bioavailability (%)	60	B
Fraction Unbound (f_u)	0.35	B
P-gp Vmax (µM/sec)	0.028	C
P-gp Km (µM)	43.93	C
CYP1A1 Vmax (nmol/min/nmol of enzyme)	4.6	A
CYP1A1 Km (µM)	61.4	A
CYP3A5 Vmax (nmol/min/nmol of enzyme)	4.7	A
CYP3A5 Km (µM)	312	A
Renal clearance (l/h/Kg)	0.52	D

	Vd (l/kg)	4.2	D

A- ADMET Predictor 9.5

B- Drugbank.ca https://www.drugbank.ca/drugs/DB00889

C- *In-vitro* Caco2 cells results, optimized by MembranePlus to: P-gp V_{max} 0.035 µM/sec and P-gp Km 49.1 µM

D- Is from reference (Roche, 2013)

Table 7-2. Comparing values from ADMET and literature.

Value	ADMET	Literature	Reference
Mwt (g/mol)	312.41	312.417	https://www.drugbank.ca/drugs/DB00889
Solubility (mg/ml) pH=7	17	18	SciFinder
LogP	2.2	2.55, 2.8	https://doi.org/10.1016/j.jconrel.2014.05.022, SciFinder, respectively
pKa	9.21	9.01, 10.1	https://www.drugbank.ca/drugs/DB00889, SciFinder, respectively

Development of a PBPK model for granisetron using GastroPlus

We also used GastroPlus to develop and validate granisetron plasma and brain profiles, using parameters obtained from MembranePlus and literature values from different formulations (Oral, IV, SubQ, and transdermal). It was also used to predict the differences in granisetron levels in both plasma and brain in response to genetic variations in granisetron metabolizing enzymes CYP1A1 and CYP3A5.

The general workflow of granisetron PBPK model development and validation involved the following steps. Granisetron physicochemical properties and metabolism data were acquired from the literature or estimated by ADMET Predictor. A summary of these parameters is listed in Table 7. The model was validated by comparing the predicted PK data with observed data from the literature. The predicted mean values of the PK parameters C_{max} and AUC were then obtained based on the simulations. Besides C_{max} and AUC, verification of the established PBPK models was based on T_{max}, V_d, CL and $t_{1/2}$.

Concentration-time profiles based in the literature were used and validated for four different granisetron formulations (oral, IV, SC and transdermal) (Gurpide *et al.*, 2007*a*; Mason *et al.*, 2012; Zhao *et al.*, 2016; Spartinou *et al.*, 2017) by scanning with GetData Graph Digitizer (version 2.26; http://getdata-graph-digitizer.com). Physiological values for intestinal volumes, lengths, and pH in humans used were those built in the software, except for the transdermal forms of granisetron. Transdermal granisetron is available as a matrix-type patch;however, GastroPlus does not offer this formulation, but it has a reservoir-type patch, and recommends using a transdermal solution to simulate matrix- type patch. Thus, in this work, for transdermal granisetron, a transdermal solution was used.

The transdermal model in GastroPlus consists of the following layers in the order of: a) stratum cornium with 10 sublayers and a thickness of 13.03 microns, b) viable epidermis layer with 5 sublayers and 61.43 microns in thickness, c) dermis with 5 sublayers and 1130.6 microns of thickness and 9.89 ml/min/100g skin blood flow rate, and d) the subcutaneous layer with 2641.8 microns thickness, 2.6 ml/min/ 100gsubQ blood flow rate (Zhao *et al.*, 2016). Both the dermis and the subQ tissues are linked with the systemic circulation; however, only the subQ tissue is linked to the lymphatic circulation (Suehiro *et al.*, 2016). Granisetron patch is applied to the stratum cornium. Three doses of granisetron patches have been validated (34.3 with a surface area of $52cm^2$, 21.8 with a surface area of $33cm^2$ and 9.9 mg with a surface area of $15cm^2$) with an application time of 168 hours. Evaporation was not considered since the compound is not volatile.

CYP1A1 and CYP3A5 polymorphisms and granisetron variability

The most important benefit of using PBPK modeling is the ability to predict PD parameters by connecting granisetron plasmas or tissue concentrations to its possible concentration at the site of action, thus being able to predict granisetron effect. (Perera *et al.*, 2013). That is important because plasma concentration cannot be used directly as a substitute for the concentration at the site of drug action (Chetty *et al.*, 2014). An additional benefit of this method is that it possibly lets us inspect the effect of variability in various physiological factors (e.g., genetic polymorphisms) on the drug effect, particularly where clinical studies are lacking (Perera *et al.*, 2013).

Granisetron is mainly metabolized to 7-hydroxygranisetron and, to a lesser degree, to 9-desmethyl granisetron by CYP1A1 and CYP3A (Corrigan *et al.*, 1999; Nakamura *et al.*, 2005; Sissung *et al.*, 2011; Zoto *et al.*, 2015). Single nucleotide polymorphisms (SNPs) in CYP3A and CYP1A1 genes can affect drug metabolism. For instance, the allele variant CYP1A1*2A is associated with increased enzymatic activity (extensive metabolizer, EM), while the allele variant CYP3A5*3 is associated with decreased enzymatic activity (poor metabolizer, PM) (Bustos *et al.*, 2016). To study the effect of CYP1A1 and CYP3A5 polymorphisms on granisetron plasma and brain levels, GastroPlus which offers both enzymes as PM (CYP3A5*3) and EM (CYP1A1*2A) will be used to test whether polymorphisms in these enzymes could affect granisetron levels and consequently the effect on nausea and vomiting. From observed and predicted plasma vs. time profiles, granisetron brain concentrations, and hence 5-HT3 receptor occupancy, were predicted in both CYP1A1*2A and CYP3A5*3 carriers.

Granisetron brain levels were predicted based on the partitioning between the plasma and the brain (kp). For 5-HT3 receptors occupancy prediction, data from reference (Endo *et al.*, 2012) following granisetron 2 mg oral was used by correlating brain concentrations to occupancy. Direct

response model was used in the pharmacodynamic simulation, where this model has its theoretical

roots in receptor-binding theory, as shown in equation 1:

$$E = E_0 + (\frac{E_{max} C}{EC_{50} + C}) \qquad\qquad (Equation\ 1)$$

Where E_0 is the baseline response, E_{max} is the maximum response and EC_{50} is the

concentration at which 50% of the maximum response is observed. E_{max} and EC_{50} were calculated

from concentration vs. occupancy plot using GraphPad software, where the EC_{50} value was

0.97µM. To have a good response to CINV, granisetron needs to occupy at least 75% of 5-HT3

receptors (Corrigan *et al.*, 1999).

Statistical analysis

The experimental results were statistically analyzed for significant differences using two-tailed

Student's t-test. A p-value <0.05 was considered statistically significant. Results from in vitro

studies were expressed as mean ± SD. All studies were performed at *n*=3.

Results

HPLC Method validation

The linearity of the method was evaluated by preparing six series of standard solutions of

granisetron in the range of 0.5-50 (0.5, 1, 5, 10 and 50) µg/ml in acetonitrile and injection of the

solutions to the HPLC system. Excellent correlation between granisetron peak area and

concentration was observed with $r^2 > 0.999$. Statistical data are presented in Table 8.

The accuracy and precision of the method was evaluated at three different concentrations of

granisetron (0.5, 5, and 50 µg/ml) in triplicate and during the three separate days. Concentrations

were determined, using calibration standard curves prepared for each day. The within-day and

between-day data are presented in Table 9. The robustness of the method was determined by

evaluating the influences of small changes in the mobile phase composition, and buffer

concentration. Peak area values were influenced less than ± 3% in all different conditions used.

The retention time of granisetron changed about 7% using different mobile phase composition. .

Chromatograms for granisetron stability are shown in Figure 6. The LOQ is the lowest

concentration in the calibration curve that give reliable levels with CV <20% was found to be 0.5

µg/ml for granisetron. An estimate of limit of detection LOD is the lowest analyte concentration

likely to be reliably distinguished, based on S/N ratio of 3 was found to be 0.05µg/ml. The

relative recovery of granisetron from media at three different concentration levels by standard

addition method ranged from 99.5 to 100.7%.

Table 8. Linearity data of calibration curves of granisetron.

Parameter	Values
Linearity range	0.5-50 µg/ml
Linearity equation	y= 21.16x-1.46
Correlation coefficient (r^2)	0.9997

Table 9. Inter and intra-day precision and accuracy of the method for determination of

granisetron (Three sets for 3 days).

| Concentration (µg/ml)	Concentration measured (µg/ml)	Precision%	Accuracy%
Inter-day			
0.5	0.502	2.85	1.2
5	5.1	1.25	0.52
50	49.91	0.85	0.41
Intra-day			
0.5	0.505	2.52	1.5
5	5.04	1.87	0.3
50	49.94	0.95	0.68
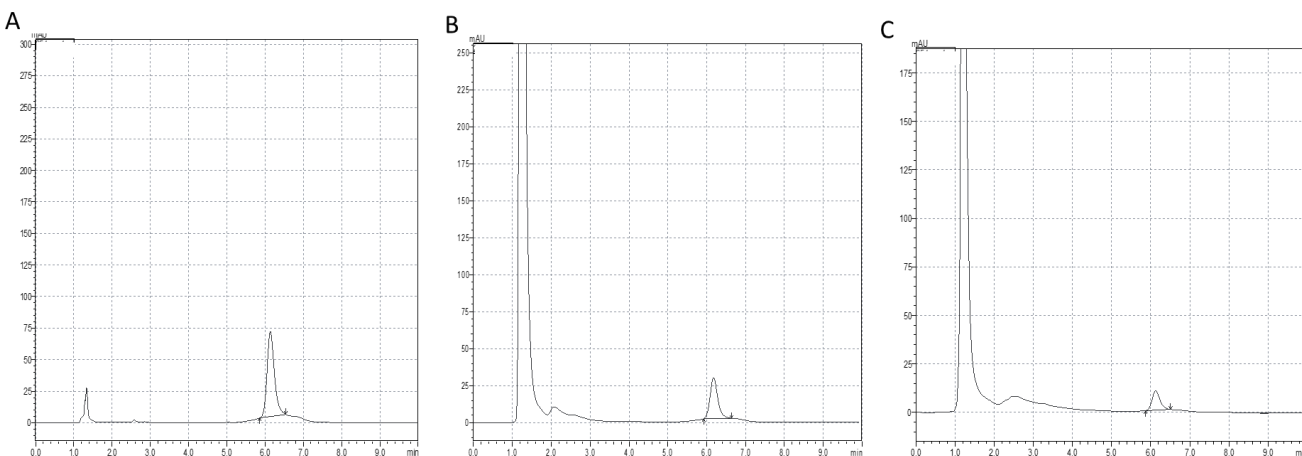
Figure 6. Representative chromatograms from HPLC analysis for granisetron. (A) Granisetron dissolved in mobile phase injected directly after preparation (B) Sample of Granisetron from transport study (C) Granisetron recovery from media samples, where the concentration added to the sample was 5 µg/ml and the concentration measured was 5.0±0.07 µg/ml.

Prediction and validation of granisetron transport across Caco2 monolayer and the use of *In-vitro* transport studies to calculate the efflux ratio and Michalis-Menten parameters

First, we had to validate the expression of P-gp in Caco2 cells used for transport studies using western blot. As seen in Figure 7A, where we can see a significant increase in the expression of P-gp going up with passages number in Caco2 cells. We also validated cell viability of Caco2 over several concentrations of granisetron (10-400 µM), as shown in Figure 7B, where we notice that there is no significant change in cell viability over the concentration range used of granisetron.
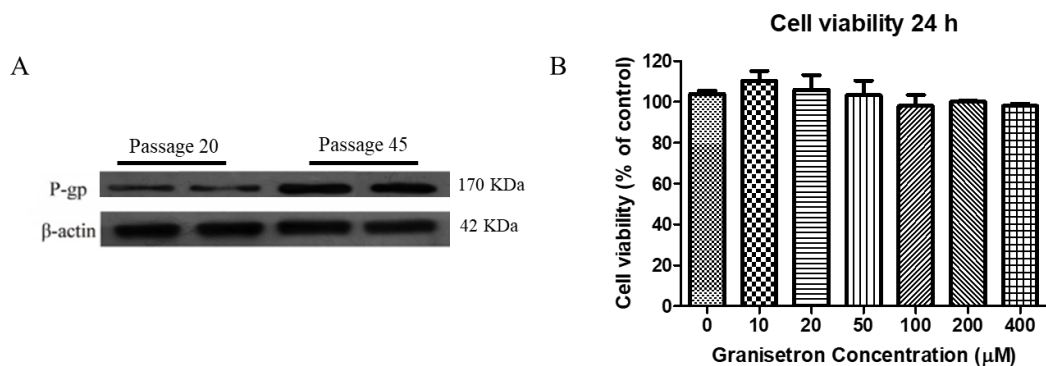
Figure 7. A. P-gp expression in Caco2 cells at passage 20 and passage 45. The picture shows a significantly higher P-gp expression in passage 45 number of Caco2 cells, which was used in all *in-vitro* experiments. **B.** MTT assay was used to assess cell viability. Control cells were incubated in granisetron free media in parallel to treatment groups.

Michalis –Menten kinetic constants V_{max} and K_m were determined from granisetron transport with time from A→B over the concentrations range 10-400 µM as seen in Figure 8. Values were 0.028 µM/sec for V_{max} and 43.93 µM for K_m. These values were optimized by MembranePlus to: P-gp Vmax 0.035 µM/sec and P-gp Km 49.1 µM to predict and validate granisetron transport and permeability across Caco2 cells monolayer. We were also able to predict the intracellular Km of 20 µM. Saturation was obtained in the range from 100 to 400 uM. Data was analysed and confirmed using two softwares: Desmos and GraphPad. Figure 8A shows that data analysis obtained by Desmos (Vmax= 0.024 µM/sec and Km is=48.2 µM), is similar to that obtained using Graphpad (where Vmax is=0.028 µM/sec and Km is 43.9 µM).
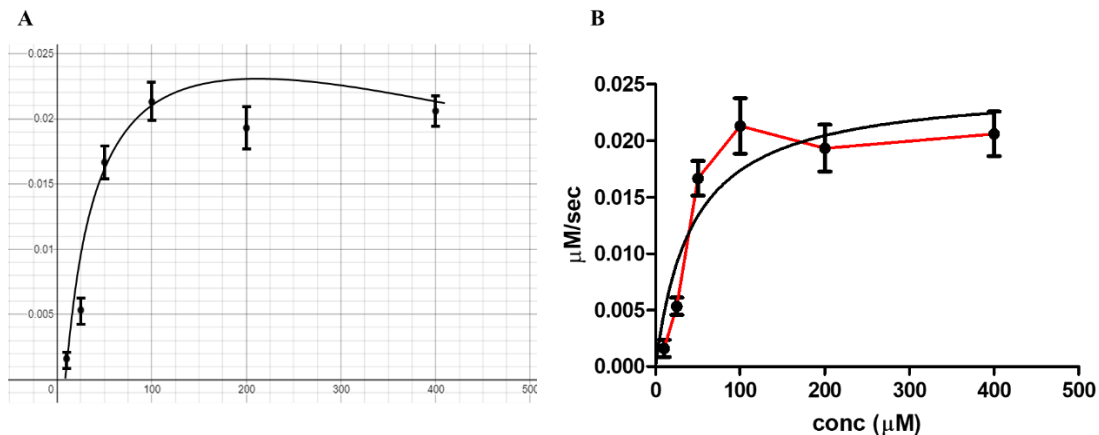
Figure 8. Michalis-Menten profile to calculate Vmax and Km values from *in-vitro* transport studies. **A** Using the software Desmos. **B.** Using Graphpad. The black curves represent the virtual non-linear regression lines predicted by both software, while the red line is the connecting line between dots. Saturation is noticed in both figures. The flux is plotted against several concentrations of granisetron till saturation is reached. **A.** Vmax value is 0.024 µM/sec, and Km value is 48.2 µM. **B.** Vmax value is 0.02813 µM/sec and Km value is 43.93 µM.

Using the input parameters that are listed in Table 7-1, we were able to validate the transport of granisetron across Caco2 cell monolayer from apical to basolateral (A➔B) and basolateral to the apical (B➔A) sides in the presence and absence of verapamil (a P-gp inhibitor) and bafilomycin A1 (increase lysosomal pH) and are present in Figure 9 (Tapper and Sundler, 1995). Apparent permeability (Papp) and efflux ratios were calculated as follow:

$$Papp = (\frac{dCr}{dt})(\frac{Vol}{Cd*A}) \hspace{3cm} (Equation\ 2)$$

Where: Cr = concentration in the receiving compartment, t= time (sec), Vol=volume in the receiving compartment (ml), Cd=concentration in the donor compartment at t=0, and A= membrane surface area that is 1.131 cm².

$$Efflux\ ratio = \frac{PappB \rightarrow A}{PappA \rightarrow B} \hspace{4cm} (Equation\ 3)$$

Where: Papp$_{B \rightarrow A}$= permeability from B→A, and Papp$_{A \rightarrow B}$= permeability from A→B.
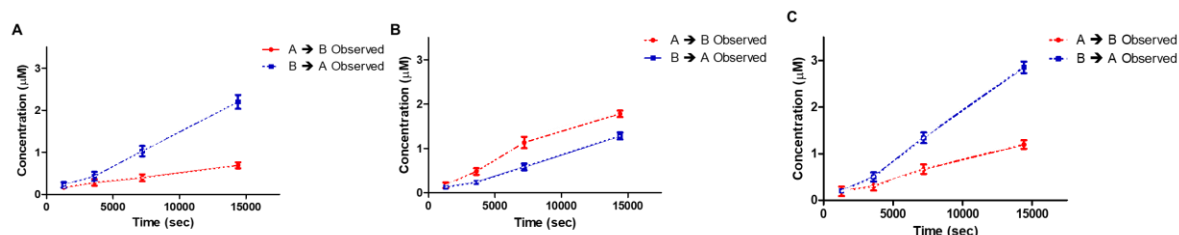
Figure 9. Calculated granisetron transport across Caco2 monolayer. **A.** Granisetron transport across Caco2 cell monolayer from apical side to basolateral side (A→ B) (red line) and from basolateral side to apical side (B → A) (blue line). **B.** Granisetron transport across Caco2 cell monolayer from in the presence of verapamil. **C.** Granisetron transport across Caco2 cell monolayer in the presence of bafilomycin A1.

Figure 10A shows the differences in the permeability of granisetron in the presence and absence of verapamil as a P-gp inhibitor. In the absence of verapamil, the permeability of granisetron was significantly higher ($p<0.005$) from B→ A, indicating the presence of P-gp as a limiting factor for permeability. Efflux ratios ≥ 2 demonstrate that a drug is a P-gp substrate, (Dolghih and Jacobson, 2013) and data shown in Figure 10A suggest granisetron is a P-gp substrate where in the absence of verapamil, granisetron efflux ratio was 3.0 that dropped to 0.9 with verapamil and in the presence of bafilomycin A1 with an efflux ratio 1.11. Figure 10B shows the predicted changes in granisetron permeability over a range of granisetron concentrations, where we can notice a steady behavior of the permeability followed by a sudden increase. This could be explained by the saturation of P-gp and lysosomes with higher granisetron concentration resulting in the passive diffusion of granisetron.
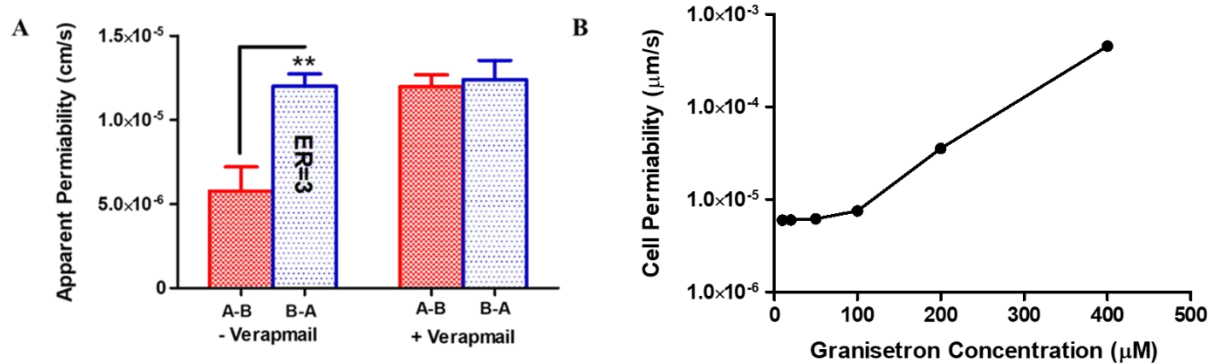
Figure 10. Calculated apparent permeability of granisetron through Caco2 cell monolayer. **A.** In the absence of verapamil where the permeability of granisetron was significantly higher from B→ A, indicating the presence of P-gp as a limiting factor for permeability. The efflux ratio in the absence of verapamil is 3, where it drops down to 0.9 in the presence of verapamil, suggesting granisetron is a P-gp substrate. **B.** Predicted granisetron cell permeability over a range of granisetron concentrations. Data are presented as mean $\pm$ SD. ** $p<0.005$.

In-vitro **determination of granisetron lysosomal entrapment**

To determine lysosomal entrapment of granisetron, cells, and media collected were analyzed using the HPLC to determine granisetron concentrations. Then, Kp was calculated from granisetron concentration in the cell in the absence or presence of NH_4Cl added to the medium. NH_4Cl prevents lysosomal entrapment by increasing lysosomal pH, and thus reduces granisetron accumulation in the lysosomes. In the absence of NH_4Cl, granisetron demonstrated intracellular accumulation (*i.e.,* in the lysosomes) as suggested by the high Kp value (Figure 11A), which was significantly ($p<0.005$ for the 5 and 10μM and <0.0001 for the 50 μM) reduced in the presence of NH_4Cl (which raises lysosomal pH and reduces granisetron lysosomal accumulation) due to intracellular granisetron transport to the media. In the absence of NH_4Cl, Kp increased with 10 μM granisetron that could be related to P-gp saturation and thus less efflux, as shown in Figure 11A.
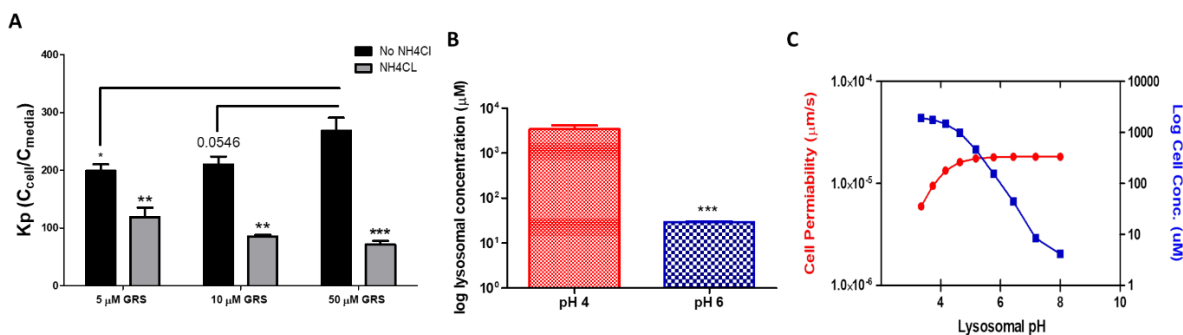
**Figure 11.** Calculated granisetron lysosomal entrapment. **A)** Observed Kp (C_{cell}/C_{media}) in the absence and the presence of 20 mM ammonium chloride (NH4Cl) at different granisetron concentrations. Ammonium chloride, that decreases lysosomal entrapment, thus decreases lysosomal pH, significantly decreased granisetron intracellular accumulation relative to control. **B)** Predicted (using MembranePlus) lysosomal entrapment of granisetron at 2 different pHs. Where at pH 4 (normal lysosomal pH), granisetron was highly entrapped inside the lysosomes and this was significantly decreased when the lysosomal pH increased to 6. **C)** Shows the predicted effect of changes in lysosomal pH on cell permeability and granisetron cell concentration. Data are presented as mean $\pm$ SD. * $p<0.05$, ** $p<0.005$, and *** $p< 0.0001$.

The assessment of P-gp effect and lysosomal entrapment using MembranePlus

To confirm lysosomal entrapment of granisetron, bafilomycin A1, a vacuolar H+ -ATPase inhibitor that reduces lysosomal acidification (Tapper and Sundler, 1995), was added to the medium simultaneously with granisetron. As shown in Figure 11B and using MembranePlus, we were able to predict that granisetron shows greater lysosomal entrapment in the absence of bafilomycin A1. In contrast, in the presence of bafilomycin A (lysosomal pH change from 4 to 6), granisetron lysosomal concentrations decreased significantly ($p<0.0001$). MembranePlus™ was also used to simulate granisetron cell permeability and intracellular concentration. Figure 11C shows the effect of changes in lysosomal pH on granisetron permeability as well as granisetron cell concentration, where we can notice that with the increase in lysosomal pH,

granisetron cell permeability increases. However, granisetron cell concentration decreases, suggesting an increase in lysosomal pH would prevent granisetron entrapment inside the lysosomes. Figure 12 shows the effect of implying P-gp and lysosomal entrapment parameters on granisetron plasma profiles, where we can notice a successful fit for observed and predicted values with the parameters (Figure 12A), a fit that was lost when the optimized parameters were not used (Figure 12B). Figure 13A shows the effect of changes in granisetron logP on Cmax values. We can notice that changes of logP that deviates from the original logP value (2.2) did not have an effect on Cmax. Figure 13B shows the effect on changes in stomach and intestinal pH on percent absorbed of granisetron. We can conclude that while the gastrointestinal pH increases there is a trend in increasing the precent absorbed of granisetron. This could be because of the increased percent unionized granisetron at the site of absorption with increasing pH.
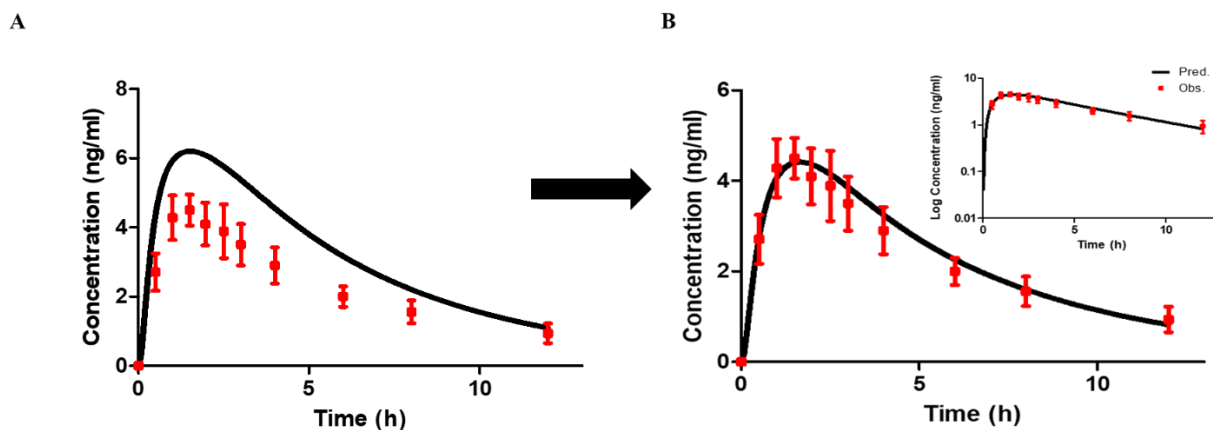
Figure 12. Granisetron plasma profile after 2mg oral with and without using refined parameters for P-gp and lysosomes. **A.** Without the parameters. **B.** Using the parameters.
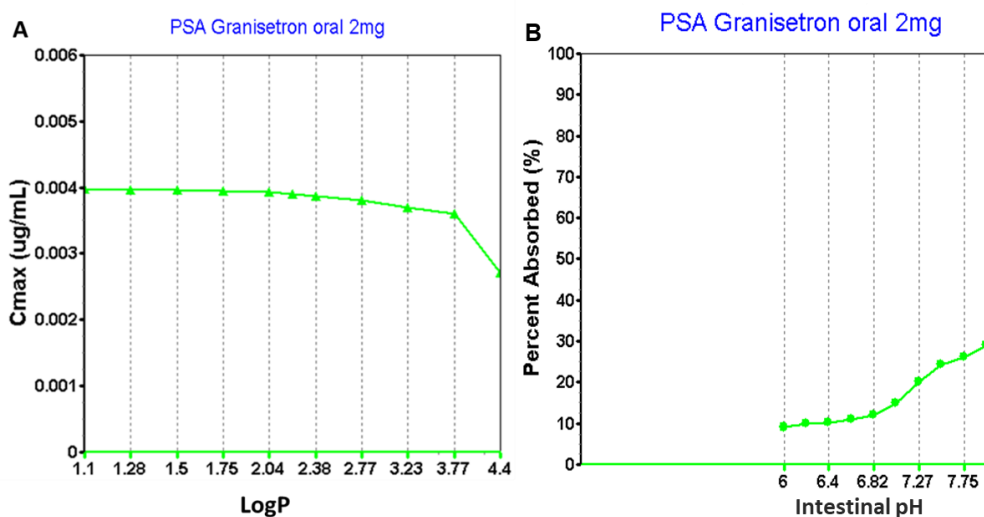
Figure 13. Parameter sensitivity analysis for the effect of the change of **A.** LogP values on granisetron Cmax. **B.** the effect of changing stomach and intestinal pH of granisetron absorption.

Development of a PBPK model for granisetron genetic variation

Input data that were used in the simulation are presented in Table 7. The model was developed and validated against granisetron disposition kinetics from four different formulations (Oral, IV, SubQ, and transdermal). The simulated plasma concentration-time profiles captured the observed PK profiles (Figure 14) and predicted values. Model-predicted C_{max}, AUC_{0-t}, V_d, and Clsys met the verification criterion, with predicted/observed ratio in the range of 0.80–1.2 and are presented in Table 10.
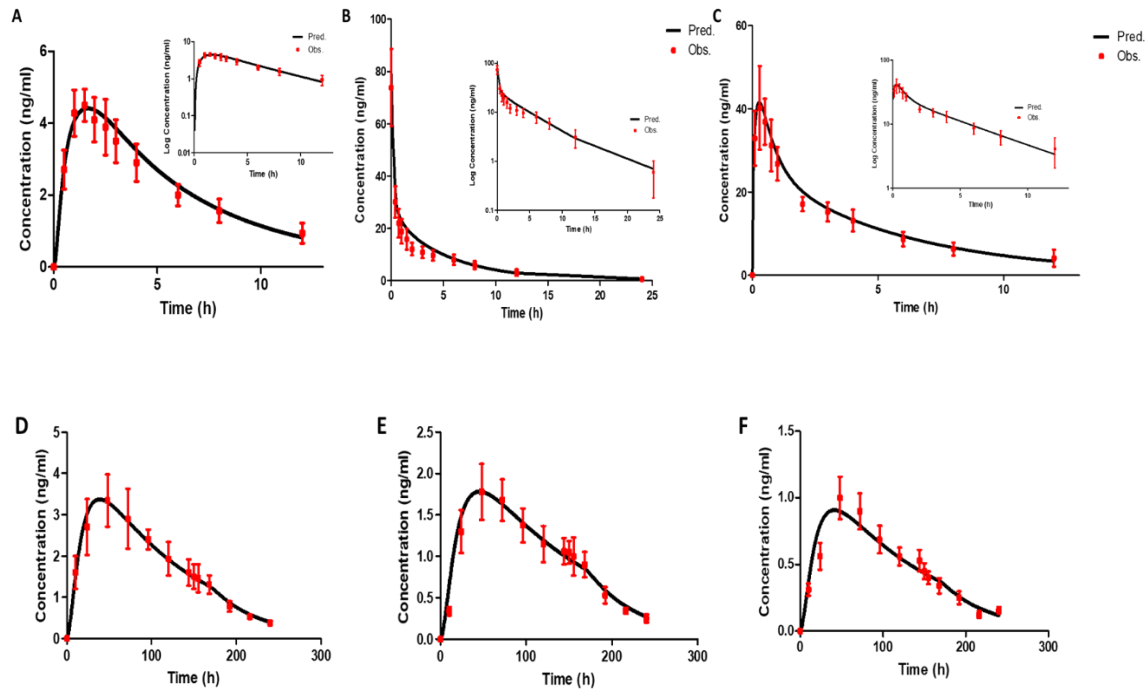
Figure 14. Predicted and observed plasma concentration-time profiles of granisetron after administration of a single 2 mg oral (A), 3 mg IV (B), and 3 mg SC dose (C). Transdermal granisetron is predicted for three different doses at (D) 34.3 mg, (E) 21.8 mg, and (F) 9.9 mg. The square symbols represent the mean of observed data, and solid lines represent the predicted mean of granisetron profiles. Inserts contain granisetron plasma profiles in a semi-log scale. Observed data for oral dose (A) is from (Zhou *et al.*, 2014), for IV (B) and SubQ (C) is from (Gurpide *et al.*, 2007*b*), the transdermal doses (D-F) are from (Howell *et al.*, 2009).

Table 10. Observed and predicted pharmacokinetic parameters of granisetron in four different formulations after a single administration (oral, IV and SC) and after 168 h of application for 3 dosages of transdermal granisetron patches. Observed data for oral dose (A) is from (Zhou *et al.*, 2014), for IV (B) and SubQ (C) is from (Gurpide *et al.*, 2007*b*), the transdermal doses (D-F) are from (Howell *et al.*, 2009).

Formulation		C_{max} (ng/ml)	T_{max} (h)	Vd (L)	Clsys (L/h)	$t_{1/2}$ (h)	AUC_{0-t} (ng*h/ml)	$AUC_{0-\infty}$ (ng*h/ml)
Oral (2mg)	Observed	4.5	1.5	301.1	36.1	6.4	27	35
	Predicted	4.41	1.6	299	35.2	5.9	28	33
	Obs/Pred	**1.0**	**0.9**	**1.0**	**1.0**	**1.1**	**1.0**	**1.1**
IV (3mg)	Observed	72.4	NA	274.1	34.2	7.1	146	150
	Predicted	82.1	0.1	280	35.2	6.1	147	164
	Obs/Pred	**0.9**	**NA**	**1.0**	**1.0**	**1.1**	**1.0**	**0.9**
SC (3mg)	Observed	43.7	0.3	218.9	35.1	7.9	128.4	NA
	Predicted	41.59	0.28	250	34.2	7.3	140	169.28
	Obs/Pred	**1.1**	**1.1**	**0.9**	**1.0**	**1.1**	**0.9**	**NA**
Transdermal 52 cm^2	Observed	3.23	46	NA	NA	35.9	NA	420
	Predicted	3.36	41	310	36.5	38	451	460
	Obs/Pred	**1.0**	**1.1**	**NA**	**NA**	**0.9**	**NA**	**0.9**
Transdermal 33 cm^2	Observed	1.78	48	NA	NA	30.9	NA	287
	Predicted	1.68	45.8	310	36.5	38	253	271
	Obs/Pred	**1.1**	**1.0**	**NA**	**NA**	**0.8**	**NA**	**1.1**
Transdermal 15 cm^2	Observed	1	48	NA	NA	30.9	NA	149
	Predicted	0.9	42	310	36.5	38	127	135
	Obs/Pred	**1.1**	**1.1**	**NA**	**NA**	**0.8**	**NA**	**1.1**

CYP1A1 and CYP3A5 polymorphism and granisetron variability

Figure 15 shows the predicted effect of CYP1A1 and CYP3A5 polymorphism on granisetron levels in the plasma and the brain after 2mg oral granisetron. GastroPlus offers a form of extensive and poor metabolizer settings of CYP enzymes. These were applied for CYP1A1 and CYP3A5 enzymes. To have a good response to CINV, granisetron needs to occupy at least 75% of 5-HT3 receptors (Corrigan *et al.*, 1999). Figure 15A-C and Table 3 show that CYP1A1*2A polymorphism decreased significantly ($p<0.005$ for AUC, and $p< 0.0001$ for brain and plasma) granisetron levels in plasma and brain, and $AUC_{0-\infty}$ when compared to CYP1A1*1 (wild type). CYP3A5*3 polymorphism (Figure 15D-F), on the other hand, increased significantly ($p< 0.0001$) granisetron plasma levels in plasma and brain, and $AUC_{0-\infty}$ when compared to CYP3A5*1 (wild type).
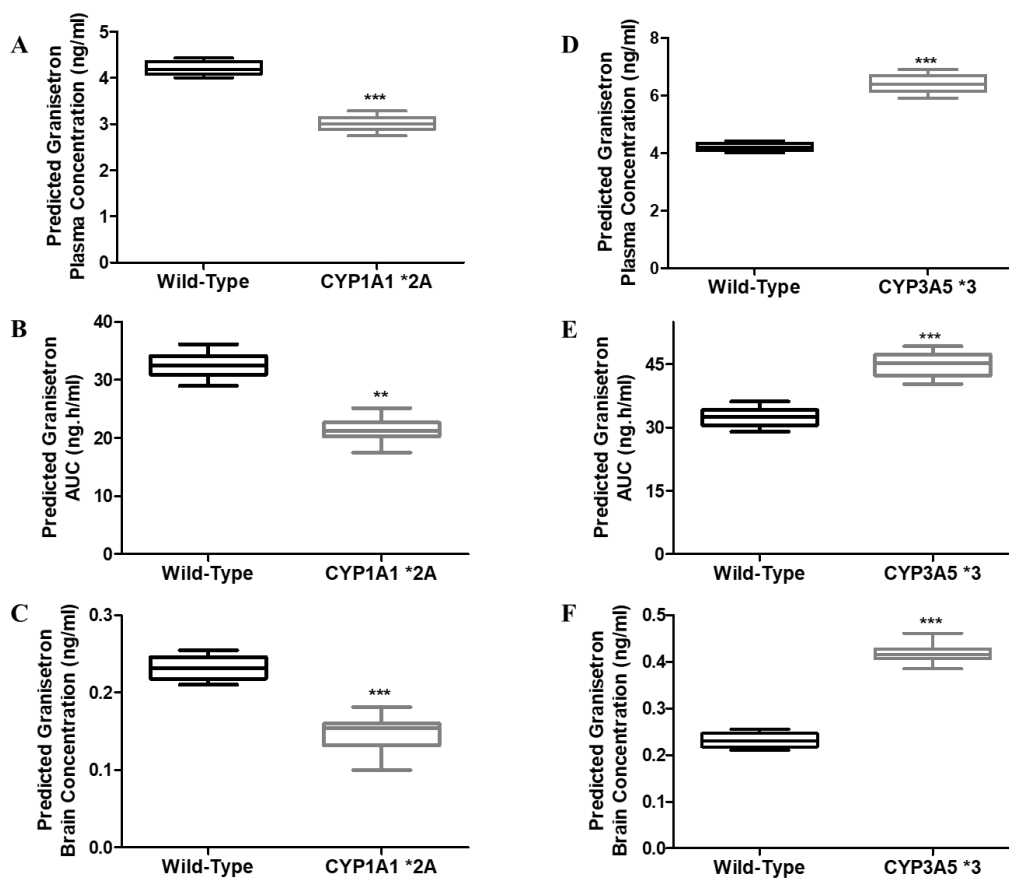
Figure 15. The effect of CYP1A1 and CYP3A5 polymorphisms on granisetron variability. (A-C) granisetron plasma (A), $AUC_{0-\infty}$ (B) and brain levels (C) are significantly decreased in the presence of CYP1A1 SNP polymorphism namely CYP1A1*2A. (D-F) granisetron plasma (D), $AUC_{0-\infty}$ (E) and brain levels (F) are significantly increased in the presence of CYP3A5 SNP polymorphism namely CYP3A5*3. ** $p<0.005$, and *** $p< 0.0001$.

Table 11 shows predicted and observed PK parameters in wild-type patients and predicted PK and PD parameters for CYP1A1*2A and CYP3A5*3 polymorphisms. Predicted/observed ratio for wild-type C_{max}, $AUC_{0-\infty}$ and T_{max} were within the acceptable prediction range of 0.8-1.2. Predicted brain concentration was decreased in CYP1A1*2A compared to wild-type, where receptor occupancy decreases, which could result in less control of the CINV. Conversely predicted brain concentration were increased in CYP3A5*3 compared to

wild-type, where receptor occupancy increased significantly, which results in better control of the CINV with this polymorphism. Our model predicted a receptor occupancy of 71% in wild-type. However, the occupancy of granisetron is predicted to decrease to 62% in patients who have CYP1A1 *2A SNP and to increase to 92% in patients who have CYP3A5 *3 SNP.

Table 11. Predicted PK and PD parameters in CYP1A1*2A and CYP3A5*3 compared to observed and predicted parameters in wild type after a 2mg PO granisetron. Observed data from (Corrigan *et al.*, 1999; Spartinou *et al.*, 2017).

PK/PD parameters	Wild-type			CYP1A1 *2A	CYP3A5 *3
	Observed	Predicted	Obs/Pred	Predicted	Predicted
C_{max} (ng/ml)	4.5±0.55	4.41	1.02	2.91	6.17
AUC $_{0-\infty}$ (ng-h/ml)	34.69±0.82	33.43	1.03	21.57	46.02
T_{max} (h)	1.5±0.02	1.6	0.93	1.6	1.6
Brain Conc. (ng/ml)	NA	0.37	NA	0.2	0.55
Receptor occupancy %	70-90%	71	--	62	98

Discussion

Part 1 (P-gp and lysosomes):

Previous models have been developed for granisetron (Moura, 2011; Xia *et al.*, 2013; Elmorsi *et al.*, 2016; Dallmann *et al.*, 2018). In these studies, models were developed to predict granisetron PK from oral and IV formulations (Moura, 2011; Xia *et al.*, 2013; Elmorsi *et al.*, 2016; Dallmann *et al.*, 2018). Here, we successfully predicted granisetron profiles and PK parameters for oral and IV formulations as well as for transdermal patches. We also were able to successfully predict the effect of P-gp and lysosomes on granisetron permeability, the effect of genetic polymorphisms in CYP1A1, and CYP3A5 enzymes on granisetron disposition (Perrine Susan, 2005; Faria *et al.*, 2014; Gilmore *et al.*, 2018). We were also able to correlate granisetron plasma and brain concentrations to its receptor occupancy, where higher occupancy would result in better CINV control.

MembranePlus® was used to develop a model for granisetron to analyze *in-vitro* permeability that is responsible for mechanisms engaged to observed apparent permeability such as transport and drug accumulation in some intracellular compartments (e.g., lysosomes) (Lipper and Higuchi, 1977; Adson *et al.*, 1995; Heikkinen *et al.*, 2009). In this work, MembranePlus® was used to predict granisetron concentration-time profiles in the apical and basolateral compartments after administration of granisetron in the presence of bafilomycin A1 and verapamil. Figure 1 shows the observed and predicted transport of granisetron in both directions across the monolayer in the presence and absence of bafilomycin A1 and verapamil, using input parameters presented in Table 7. The developed model was used to predict the effects of lysosomal trapping of granisetron on the measured permeability. MembranePlus® has facilitated

the analysis of *in-vitro* experiments taking into consideration the variety of mechanisms such as P-gp efflux and lysosomal trapping, affecting measured apparent permeability (Szeto *et al.*, 2007). The current study shows that it is a promising tool in drug research and development, not only for predicting of granisetron permeability but also in other elements that affect drug distribution in several tissues (e.g., lysosomal trapping) (Adson *et al.*, 1995).

Serotonin released from the enterochromaffin cells of the small intestines after the chemotherapeutic agent's administration activates both central and peripheral 5-HT3 receptors. Central structures (area postrema) are rich with 5-HT3 receptors. Granisetron suppresses CINV by inhibiting serotonin binding to 5-HT3 receptors (Kioka *et al.*, 1989; Andrews, 1992; Darmani, 1998; Zhong *et al.*, 2014). P-gp restricts the permeability of drugs from the apical side of intestinal lumen and blood–tissue barriers. P-gp identifies and effluxes a variety of structurally and biochemically irrelevant substrates (cyclic, linear, basic, uncharged, zwitterionic, negatively charged, hydrophobic, aromatic, nonaromatic, amphipathic) from 250 to 4000 molecular weight (Miller *et al.*, 2009). This suggests that P-gp has a major impact on the disposition of P-gp substrates. Findings from the in vitro experiments suggested granisetron is a substrate for P-gp, consistent with other members of 5-HT3 antagonists, such as ondansetron and ramosetron, known P-gp substrates, and have chemical structure similarities (Hodges, 2011; Bustos *et al.*, 2016). The cause of the resistance to antiemetic prophylaxis with 5-HT3 receptor antagonists has been suggested to be linked to increased efflux transport by P-gp, thus decreasing its absorption (Tsuji *et al.*, 2013).

As a result of their lysosomotropic tendencies, granisetron has a distinctive PK properties including a relatively long-terminal elimination half-life (Gong *et al.*, 2007). Besides having a long-elimination half-life, there is often an extreme intra and inter- patient variability in plasma

and target levels, which could lead to wrongful dosage regimens that could possibly lead to unwanted adverse reactions or even drug-related toxicity with the lack of therapeutic effect. Granisetron shows a large volume of distribution due to its physicochemical properties and lysosomal entrapment (Daniel and Wójcikowski, 1997). The high volume of distribution indicates that most of the drug is located in the tissue (Daniel and Wójcikowski, 1997). Given that granisetron has the recognized common properties of lysosomotropic agents, such as a LogP > 1 and a basic pKa between 6.5 and 11, it could be sequestered in the lysosomes. Caco2 cell permeability assay with the assumption of a lysosomal pH of 4 was used. In Figure 11B, at a lysosomal pH = 4.0, the simulated lysosome concentration of granisetron is approximately three orders of magnitude higher than with the lysosomal pH = 6 ($p<0.0001$). The concentration of granisetron in the lysosomal compartment is reduced suggesting that granisetron, and due to its physicochemical properties, was in the cationic form when the lysosomal pH was at 4. However, when the lysosomal pH increased to 6, a greater portion of the total granisetron concentration returned to the neutral form and was able to escape the lysosomes. We can notice that the difference in LogP and pKa values from ADMET® predictor to literature values (Table7-2) did not affect Cmax and percent absorbed of granisetron as shown in Figure 13.

P-gp is present on the luminal side of the enterocytes. P-gp effluxes substrates out of the enterocytes, thus reducing substrates absorption. When granisetron is uptaken by the cells, P-gp will efflux it back to outside the cell. When P-gp is saturated, granisetron will pass the cell membrane and face the lysosomes that will engulf into the acidic environment and become and trapped in the ionized state inside the lysosomes for degradation. Granisetron that is not degraded by the lysosomes, is released and effluxed out of the cell by P-gp. Results from the transport studies (Figure 9) suggest that granisetron transport from B to A side was higher than

granisetron transport from A to B side in the absence of P-gp inhibitor verapamil (Figure 9A)

with an efflux ratio of 3; and in the presence of bafilomycin A1 with an efflux ratio 1.11 (Figure

9C); in the presence of verapamil (Figure 9B), granisetron efflux ratio dropped down to 0.9.

With Kp values presented in Figure 11A, we can conclude that in the absence of NH4Cl, Kp was

high, indicating that granisetron accumulation was predominantly intracellular. However, when

NH4Cl was added, Kp values decreased significantly ($p<0.005$ for the 5 and 10µM and <0.0001

for the 50 µM), suggesting that lysosomal pH increased, thus releasing granisetron out of the

cells into the media. This was also confirmed when we predicted lysosomal concentration of

granisetron in Figure 11B, where it shows that in the absence of bafilomycin (lysosomal pH at

4), lysosomal concentration of granisetron was significantly higher ($p<0.0001$) than when the

lysosomal pH increased to 6 (in the presence of bafilomycin).

Collectively, these results suggest granisetron transport is not only P-gp dependent, but also it is

dependent on lysosomal entrapment that could impact granisetron transport across the cell

membrane. It could be possible that the passage of granisetron from the A to the B in the

presence of lysosomal entrapment reduces the trafficking on P-gp.

Part 2 (Genetic variation):

To explain the observed variability in granisetron disposition and efficacy, we tested the

effect of genetic variation in granisetron metabolizing enzymes on its PK parameters. There are

relatively high percentages of people carrying the SNPs in CYP enzymes where these SNPs

could affect drug metabolism, ranging from 29.31% for CYP1A1*2A to 62.14% for CYP3A5*3

(Bustos *et al.*, 2016). Using PBPK, we were capable of predicting the effect of SNP in CYP1A1

and CYP3A5 on granisetron plasma and brain levels as well as the AUC. Since CYP1A1*2A is

an extensive metabolizer, granisetron levels with this polymorphism are predicted to be significantly lower ($p<0.005$ for AUC, and $p< 0.0001$ for brain and plasma). However, in the presence of the CYP3A5*3 SNP variant as a poor metabolizer, granisetron predicted plasma levels and AUC increased significantly ($p< 0.0001$) (Table 11 and Figure 15).

To show the antiemetic effect and total control over CINV, granisetron should occupy 70-90% of receptors (Spartinou *et al.*, 2017). We were able to predict the effect of SNP on the receptor occupancy of granisetron, and thus we could correlate that occupancy to the variability of granisetron effect as well as the control of CINV. We predicted that patients with CYP1A1 *2A SNP show a receptor occupancy was 62%, which could lead to less control over CINV. However, we also predicted that patients with CYP3A5 *3 SNP show a receptor occupancy of 98%, which could lead to higher control over CINV.

Conclusion

We can conclude that granisetron shows poor CINV control in around 20-30% of patients, and that could be due to several factors. Granisetron is a P-gp substrate and is usually effluxed out, thus limiting its absorption. Also, due to its physicochemical properties, granisetron gets entrapped inside the lysosomes, also limiting its passage through cell lines. The interplay between P-gp and lysosomes plays an important role in granisetron absorption and availability for the site of action. Since granisetron is mainly metabolized by CYP1A1 and CYP3A5, a SNP in these CYP enzymes has been predicted to affect granisetron PK parameters as well as receptor occupancy, thus control of CINV.

Chapter 4

Conclusions

      PBPK modeling is a useful tool to determine the strategy of drug development. PBPK modeling could be very effective in studying drugs' pharmacokinetics and pharmacodynamics in particular populations. PBPK modeling provides a platform to study the impact of genetic variations on drug pharmacokinetics and pharmacodynamics when clinical studies have not or cannot be conducted. This highlights the utility of PBPK/PD modeling and the unique application of the PBPK model to a PD outcome that could be utilized to help define potential cut-offs for caffeine intake in various stages of pregnancy. In the second chapter, our first objective was to develop and validate a non-pregnancy and pregnancy PBPK/PD model. We were able to build both models and the model successfully predicted the observed data. Following that, we built the pregnancy model taking into considerations changes that usually occur during pregnancy. We were able to verify that caffeine maternal blood levels increase with pregnancy due to progressive reduction in its metabolism by CYP1A2, since CYP1A2 is downregulated as pregnancy progresses. We were also able to predict FPC caffeine concentrations and how it accumulates over trimesters because of lack of metabolizing enzymes inside the FPC. We also correlated maternal caffeine levels with PD effect and its risk of miscarriage. We concluded that caffeine levels increase leads to reduced levels of PDE and increased levels of cAMP and epinephrine. For example, in T3, daily intake of 200 mg or more of caffeine increased epinephrine blood levels by 4-fold and higher when compared to normal levels, which could increase the risk of pregnancy loss. So, we suggest that any caffeine dose

that could result in low PDE levels and high epinephrine levels could cause the patient to miscarriage (200mg) so pregnant women are advised to limit their caffeine intake. In the third chapter, our objectives were to build a PBPK model to predict and verify the transport of granisetron over Caco2 cell monolayer, and to study the effect of P-gp and lysosomes on granisetron levels. We were also able to build a PBPK model to predict the effect of genetic variations on granisetron levels. Our conclusions were that granisetron is a P-gp substrate and is usually effluxed out thus limiting its absorption. Due to its physiochemical properties, granisetron gets entrapped inside the lysosomes also limiting its passage through cell lines. We also concluded that SNP in CYP1A2 and CYP3A5 could hugely affect granisetron plasma as well as brain levels; thus, eventually affects receptor occupancy and the ability to control CINV. Our future directions will be to use PBPK modeling to build models and predict drug effect and doses in several other important populations like the pediatric population, where drug dosing is problematic. Another important direction is the utilization of PBPK modeling in simulating several DDI, especially in geriatric population where most of the patients are on polypharmacy and the possibility of DDI is high.

References

Aapro M, Jordan K, Feyer P. Pathophysiology of Chemotherapy induced Nausea and Vomiting [Internet]. Springer Healthc 2015Available from: http://ime.springerhealthcare.com/wp-content/uploads/Pathophysiology_CINV.pdf%0Awww.springerhealthcare.com

Abduljalil K, Furness P, Johnson TN, Rostami-Hodjegan A, Soltani H. Anatomical, Physiological and Metabolic Changes with Gestational Age during Normal Pregnancy. Clin Pharmacokinet 2012; 51: 365–396.

Adson A, Burton PS, Raub TJ, Barsuhn CL, Audus KL, Ho NFH. Passive diffusion of weak organic electrolytes across Caco-2 cell monolayers: Uncoupling the contributions of hydrodynamic, transcellular, and paracellular barriers. J Pharm Sci 1995; 84: 1197–1204.

Aldridge A. Disposition of caffeine during and after pregnancy.pdf. 1981

Alqahtani S, Kaddoumi A. Development of physiologically based pharmacokinetic/Pharmacodynamic model for Indomethacin disposition in pregnancy. PLoS One 2015; 10: 1–18.

Anderson PO. Modeling Drug Passage into Breastmilk. 2016

Andrews PLR. Physiology of nausea and vomiting. Br J Anaesth 1992; 69

Avram Goldsten. Passage of caffeine into human gonadal and fetal tissue. Aging (Albany NY) 1961: 166–168.

Badhan RKS, Chenel M, Penny JI. Development of a Physiologically-Based Pharmacokinetic Model of the Rat Central Nervous System. 2014: 97–136.

Baldwin SJ, Clarke SE, Chenery RJ. Characterization of the cytochrome P450 enzymes involved in the in vitro metabolism of rosiglitazone. Br J Clin Pharmacol 1999; 48: 424–432.

Barry Carter. Theophylline_Clearance_During_Pregnancy. 1986

Berezhkovskiy LM. Determination of Volume of Distribution at Steady State with Complete Consideration of the Kinetics of Protein and Tissue Binding in Linear Pharmacokinetics. 2004; 93: 364–374.

Bi Y, Kazolias D, Duignan DB. Use of Cryopreserved Human Hepatocytes in Sandwich Culture to Measure Hepatobiliary Transport ABSTRACT : 2006; 34: 1658–1665.

Birkett D, Miners J. Caffeine renal clearance and urine caffeine concentrations during steady state dosing. Implications for monitoring caffeine intake during sports events. Br J Clin Pharmacol 1991; 31: 405–408.

Blanchard J. The Absolute Bioavailability of Caffeine in Man. Eur J Clin Pharmacol 1983

Bolomey AA, Schreiner GE, Henry D, Bolomey BYAA, Michie AJ, Michie C, et al. SIMULTANEOUS MEASUREMENT OF EFFECTIVE RENAL BLOOD FLOW AND CARDIAC OUTPUT IN RESTING NORMAL SUBJECTS AND PATIENTS WITH ESSENTIAL HYPERTENSION Find the latest version : SIMULTANEOUS MEASUREMENT OF EFFECTIVE RENAL BLOOD SUBJECTS AND PATIENTS WITH ESSEN-. 1949; 28: 10–17.

Boulenc X, Barberan O. Metabolic-based drug-drug interactions prediction , recent approaches for risk assessment along drug development. 2011; 26: 147–168.

Braizer JL. Pharmacokientics of caffeine during and after pregnancy. 1983

Brown RP, Delp MD, Lindstedt SL, Rhomberg LR, Beliles RP. PHYSIOLOGICAL PARAMETER VALUES FOR PHYSIOLOGICALLY BASED PHARMACOKINETIC MODELS. 1997: 407–484.

Bukowski J, Korn L, Wartenberg D. Correlated Inputs in Quantitative Risk Assessment : The Effects of Distributional Shape. 1995; 15: 215–219.

Bustos ML, Zhao Y, Chen H, Caritis SN, Venkataramanan R. Polymorphisms in CYP1A1 and CYP3A5 Genes Contribute to the Variability in Granisetron Clearance and Exposure in Pregnant Women with Nausea and Vomiting. Pharmacotherapy 2016; 36: 1238–1244.

C. Ghobadi. Application of a Systems Approach to the Bottom-Up Assessment of Pharmacokinetics in Obese Patients. 2011: 1–14.

Campion EW. The Effect of Age on Serum Albumin in Healthy Males : Report From the Normative Aging Study. Bri Jou Clin Pharm 1990; 43: 18–20.

Campion EW. The effect of age on o0l-acid glycoprotein. Bri Jou Clin Pharm 1990

Center for Drug Evaluation and Research (CDER) F and DA. Vladimir Nikolaevich Chernigovski. Acta Physiol Pharmacol Bulg 1977; 3: 3–5.

Center for Drug Evaluation and Research (CDER) F and DA. Physiologically Based Pharmacokinetic Analyses — Format and Content: Guidance for Industry. US Dep Heal Hum Serv 2018: 1–6.

Cheng WS, Murphy TL, Smith MT, Cooksley WG, Halliday JW, Powell LW. Dose-dependent pharmacokinetics of caffeine in humans: relevance as a test of quantitative liver function. Clin Pharmacol Ther 1990; 47: 516–24.

Chetty M, Johnson TN, Polak S, Salem F, Doki K, Rostami-hodjegan A. Physiologically based pharmacokinetic modelling to guide drug delivery in older people. Adv Drug Deliv Rev 2018; 135: 85–96.

Chetty M, Rose RH, Abduljalil K, Patel N, Lu G, Cain T, et al. Applications of linking

PBPK and PD models to predict the impact of genotypic variability, formulation differences, differences in target binding capacity and target site drug concentrations on drug responses and variability. Front Pharmacol 2014; 5: 1–29.

Chu XKK. Intracellular Drug Concentrations and Transporters: Measurement, Modeling, and Implications for the Liver. Clin Pharmacol Ther 2013; 23: 126–141.

Claire I-R. Fetal Loss Associated with Caffeine Intake Before and During Pregnancy. 1993

Colbers A, Greupink R, Litjens C, Burger D, Russel FGM. Physiologically Based Modelling of Darunavir/Ritonavir Pharmacokinetics During Pregnancy. Clin Pharmacokinet 2016; 55: 381–396.

Corrigan BW, Nicholls B, Thakrar B, Lam R, Grosse C, Alianti J, et al. Heterogeneity in systemic availability of ondansetron and granisetron following oral administration. Drug Metab Dispos 1999; 27: 110–112.

COT Statement. Committee on toxicity of chemicals in food, consumer products and the envirometn (COT), statement on teh reproductive effects of caffeine. Food Stand Agency 2001

Dallmann A, Ince I, Coboeken K, Eissing T, Hempel G. A Physiologically Based Pharmacokinetic Model for Pregnant Women to Predict the Pharmacokinetics of Drugs Metabolized Via Several Enzymatic Pathways. Clin Pharmacokinet 2018; 57: 749–768.

Daniel WA, Wójcikowski J. Contribution of lysosomal trapping to the total tissue uptake of psychotropic drugs. Pharmacol Toxicol 1997; 80: 62–68.

Darmani NA. Serotonin 5-HT3 receptor antagonists prevent cisplatin-induced emesis in Cryptotis parva: A new experimental model of emesis. J Neural Transm 1998; 105: 1143–1154.

Davis MP, Homsi J. The importance of cytochrome p450 monooxygenase CYP2D6 in

palliative medicine. Support Care Cancer 2001; 9: 442–451.

Dedrick L. to CSF and brain tissue. 2019

Dolghih E, Jacobson MP. Predicting efflux ratios and blood-brain barrier penetration

from chemical structure: Combining passive permeability with active efflux by P-glycoprotein.

ACS Chem Neurosci 2013; 4: 361–367.

Durie BGM, Dalton WS. Reversal of drug-resistance in multiple myeloma with

verapamil. Br J Haematol 1988; 68: 203–206.

Durieux. Downloaded from anesthesiology.pubs.asahq.org by guest on 01/28/2019.

Anesthesiology 1995; 31: 305–309.

Echeverri D, Montes FR, Cabrera M, Galán A, Prieto A. Caffeine's vascular mechanisms

of action. Int J Vasc Med 2010; 2010

Edginton AN, Willmann S. Physiology-Based Simulations of a Pathological Condition

Prediction of Pharmacokinetics in Patients with Liver Cirrhosis. 2008; 47: 743–752.

Edwar Kerns. Drug like properties: concepts and structures. 2001

EFSA. scientific opinion on the safety of caffeine. 2015

Einolf HJ. Comparison of different approaches to predict metabolic drug – drug

interactions. 2007

Elmorsi Y, Barber J, Rostami-Hodjegan A. Ontogeny of hepatic drug transporters and

relevance to drugs used in pediatrics. Drug Metab Dispos 2016; 44: 992–998.

EMA. Guideline on the reporting of physiologically based pharmacokinetic (PBPK)

modelling and simulation Guideline on the reporting of physiologically based pharmacokinetic (

PBPK) modelling and simulation Table of Contents. 2018; 44

Endo J, Iihara H, Yamada M, Yanase K, Kamiya F, Ito F, et al. A randomized controlled

non-inferiority study comparing the antiemetic effect between intravenous granisetron and oral azasetron based on estimated 5-HT3 receptor occupancy. Anticancer Res 2012; 32: 3939–3947.

Engel M, Smidt MP, van Hooft JA. The serotonin 5-HT3 receptor: A novel neurodevelopmental target. Front Cell Neurosci 2013; 7: 1–8.

Fahmi OA, Boldt S, Kish M, Obach RS, Tremaine LM. PREDICTION OF DRUG-DRUG INTERACTIONS FROM IN VITRO INDUCTION DATA Application of the Relative Induction Score Approach Using Cryopreserved Human Hepatocytes. 2008; 36: 1971–1974.

Faria C, Li X, Nagl N, Mcbride A. Selection in Patients with Chemotherapy- Induced Nausea and Vomiting : A Retrospective. Am Heal Drug Benefits 2014; 7: 50–58.

FDA F and DA. Clinical Drug Interaction Studies — Study Design , Data Analysis , and Clinical Implications Guidance for Industry Clinical Drug Interaction Studies — Study Design , Data Analysis , and Clinical Implications Guidance for Industry. 2017

Frayer DW. THE ECOLOGICAL IMPLICATIONS OF BODY SIZE. 2005: 340–342.

Fromm M, Kim R. Handbook of Experimental Pharmacology 201; Drug Transporters. 2011

GADDUM JH, PICARELLI ZP. Two kinds of tryptamine receptor. Br J Pharmacol Chemother 1957; 12: 323–328.

Galligan JJ. Ligand-gated ion channels in the enteric nervous system. Neurogastroenterol Motil 2002; 14: 611–623.

Gaohua L, Abduljalil K, Jamei M, Johnson TN, Rostami-Hodjegan A. A pregnancy physiologically based pharmacokinetic (p-PBPK) model for disposition of drugs metabolized by CYP1A2, CYP2D6 and CYP3A4. Br J Clin Pharmacol 2012; 74: 873–885.

Gilmore J, D'amato S, Griffith N, Schwartzberg L. Recent advances in antiemetics: New

formulations of 5HT 3 -receptor antagonists. Cancer Manag Res 2018; 10: 1827–1857.

Gong Y, Zhao Z, McConn DJ, Beaudet B, Tallman M, Speake JD, et al. Lysosomes contribute to anomalous pharmacokinetic behavior of melanocortin-4 receptor agonists. Pharm Res 2007; 24: 1138–1144.

Grant DM, Campbell ME, Tang BK, Kalow W. Biotransformation of caffeine by microsomes from human liver. Kinetics and inhibition studies. Biochem Pharmacol 1987; 36: 1251–1260.

Gurpide A, Sadaba B, Martin-Algarra S, Azanza JR, Lopez-Picazo JM, Campanero MA, et al. Randomized Crossover Pharmacokinetic Evaluation of Subcutaneous Versus Intravenous Granisetron in Cancer Patients Treated with Platinum-Based Chemotherapy. Oncologist 2007; 12: 1151–1155.

Gurpide A, Sadaba B, Martin-Algarra S, Azanza JR, Lopez-Picazo JM, Campanero MA, et al. Randomized Crossover Pharmacokinetic Evaluation of Subcutaneous Versus Intravenous Granisetron in Cancer Patients Treated with Platinum-Based Chemotherapy. Oncologist 2007; 12: 1151–1155.

Hans Lennernas. Human Intestinal Permeability. 1998; 87: 403–410.

Heikkinen AT, Mönkkönen J, Korjamo T. Kinetics of cellular retention during caco-2 permeation experiments: Role of lysosomal sequestration and impact on permeability estimates. J Pharmacol Exp Ther 2009; 328: 882–892.

Hodges L. Very important phamacogene summary ABCB1. 2011; 21: 152–161.

Holt K, Ye M, Nagar S, Korzekwa K. Prediction of tissue-plasma partition coefficients using microsomal partitioning: Incorporation into physiologically based pharmacokinetic models and steady-state volume ofdistribution predictions. Drug Metab Dispos 2019; 47: 1050–1060.

Howell J, Smeets J, Drenth HJ, Gill D. Pharmacokinetics of a granisetron transdermal system for the treatment of chemotherapy-induced nausea and vomiting. J Oncol Pharm Pract 2009; 15: 223–231.

Huang S, Abernethy DR, Wang Y, Zhao P, Zineh I. The Utility of Modeling and Simulation in Drug Development. J Pharm Sci 2013; 102: 2912–2923.

Infante-Rivard C, Fernandez A, Gauthier R, David M, Rivard G. Fetal loss associated with caffeine intake before and during pregnancy. JAMA J Am Med Assoc 1993; 270: 2940–2943.

Insler M. The health consequences of retirement. J Hum Resour 2014; 49: 195–233.

Isoherranen N, Thummel KE. Drug metabolism and transport during pregnancy: How does drug disposition change during pregnancy and what are the mechanisms that cause such changes? Drug Metab Dispos 2013; 41: 256–262.

Jahanfar S JS. Cochrane Database of Systematic Reviews Effects of restricted caffeine intake by mother on fetal, neonatal and pregnancy outcomes (Review) Effects of restricted caffeine intake by mother on fetal, neonatal and pregnancy outcomes (Review) [Internet]. 2015Available from: www.cochranelibrary.com

Jantratid E, Janssen N, Reppas C, Dressman JB. Dissolution Media Simulating Conditions in the Proximal Human Gastrointestinal Tract : An Update. 2008; 25

Jogiraju VK, Avvari S, Gollen R, Taft DR. Application of physiologically based pharmacokinetic modeling to predict drug disposition in pregnant populations. Biopharm Drug Dispos 2017; 38: 426–438.

John R.Giudicessi, BA.Michael J.Ackerman. 2013. 基因的改变NIH Public Access. Bone 2008; 23: 1–7.

Johnson TN, Boussery K, Rowland-yeo K, Tucker GT, Rostami-hodjegan A, Limited S. A Semi-Mechanistic Model to Predict the Effects of Liver Cirrhosis on Drug Clearance. 2010; 49: 189–206.

Jones HM. Basic Concepts in Physiologically Based Pharmacokinetic Modeling in Drug Discovery and Development. 2013: 1–12.

Jones HM, Barton HA, Lai Y, Bi Y, Kimoto E, Kempshall S, et al. Mechanistic Pharmacokinetic Modeling for the Prediction of Transporter-Mediated Disposition in Humans from Sandwich Culture Human Hepatocyte Data □ ABSTRACT : 2012

Jones HM, Gardner IB, Collard WT, Stanley PJ, Oxley P, Hosea NA, et al. Simulation of Human Intravenous and Oral Pharmacokinetics of 21 Diverse Compounds Using Physiologically Based Pharmacokinetic Modelling. 2011; 50: 331–347.

Jones HM, Mayawala K, Poulin P. Dose selection based on physiologically based pharmacokinetic (PBPK) approaches. AAPS J 2013; 15: 377–387.

Jones HM, Parrott N, Jorga K, Lav T. A Novel Strategy for Physiologically Human Pharmacokinetics. 2006; 45: 511–542.

Kazmi F, Hensley T, Pope C, Funk RS, Loewen GJ, Buckley DB, et al. Lysosomal sequestration (trapping) of lipophilic amine (cationic amphiphilic) drugs in immortalized human hepatocytes (Fa2N-4 cells). Drug Metab Dispos 2013; 41: 897–905.

Ke AB, Greupink R, Abduljalil K. Drug Dosing in Pregnant Women : Challenges and Opportunities in Using Physiologically Based Pharmacokinetic Modeling and Simulations CURRENT STATUS AND NEED FOR CLINICAL. 2018: 103–110.

Ke AB, Greupink R, Abduljalil K. Drug dosing in pregnant women: Challenges and opportunities in using physiologically-based pharmacokinetic modeling and simulations. CPT

Pharmacometrics Syst Pharmacol 2018: 1–8.

Ke AB, Nallani SC, Zhao P, Rostami-Hodjegan A, Isoherranen N, Unadkat JD. A physiologically based pharmacokinetic model to predict disposition of CYP2D6 and CYP1A2 metabolized drugs in pregnant women. Drug Metab Dispos 2013; 41: 801–813.

Ke AB, Rostami-Hodjegan A, Zhao P, Unadkat JD. Pharmacometrics in Pregnancy: An Unmet Need. Annu Rev Pharmacol Toxicol 2014; 54: 53–69.

Kilpatrick G. 5-HT3 receptors. Med Res Rev 1990; 12: 3615–3630.

Kilpatrick GJ, Jones BJ, Tyers MB. Identification and distribution of 5-HT3 receptors in rat brain using radioligand binding. Nature 1987; 330: 746–748.

Kioka N, Tsubota J, Kakehi Y, Komano T, Gottesman MM, Pastan I, et al. P-Glycoprotein gene (MDR1) cDNA from human adrenal: Normal P-glycoprotein carries Gly185 with an altered pattern of multidrug resistance. Biochem Biophys Res Commun 1989; 162: 224–231.

Kirkinen P, Jouppila P, Koivula A, Vuori J, Puukka M. The effect of caffeine on placental and fetal blood flow in human pregnancy. Am J Obstet Gynecol 1983; 147: 939–942.

Knight CA, Knight I, Mitchell DC, Zepp JE. Beverage caffeine intake in US consumers and subpopulations of interest: Estimates from the Share of Intake Panel survey. Food Chem Toxicol 2004; 42: 1923–1930.

Knutti R, Rothweiler H, Schlatter C. The effect of pregnancy on the pharmacokinetics of caffeine . Related information PubMed Commons. 2014; 192: 187–192.

Kuepfer L, Niederalt C, Wendl T, Schlender JF, Willmann S, Lippert J, et al. Applied Concepts in PBPK Modeling: How to Build a PBPK/PD Model. CPT Pharmacometrics Syst Pharmacol 2016; 5: 516–531.

Kwon H, Lionberger RA, Yu LX. Impact of P-Glycoprotein-Mediated Intestinal Efflux Kinetics on Oral Bioavailability of P-Glycoprotein Substrates †. 2004; 1: 455–465.

Lange ECM De. The mastermind approach to CNS drug therapy : translational prediction of human brain distribution , target site kinetics , and therapeutic effects. 2013: 1–16.

Li D-K, Ferber JR, Odouli R. Maternal caffeine intake during pregnancy and risk of obesity in offspring: a prospective cohort study. Int J Obes 2015; 39: 658–664.

Li J, Zhao H, Song JM, Zhang J, Tang YL, Xin CM. A meta-analysis of risk of pregnancy loss and caffeine and coffee consumption during pregnancy. Int J Gynecol Obstet 2015; 130: 116–122.

Lipper RA, Higuchi WI. Analysis of theoretical behavior of a proposed zero-order drug delivery system. J Pharm Sci 1977; 66: 163–164.

Lipscomb JC, Fisher JW, Confer PD, Byczkowski JZ. In Vitro to in Vivo Extrapolation for Trichloroethylene Metabolism in Humans. 1998; 387: 376–387.

Liu X, Smith BJ, Chen C, Callegari E, Becker SL, Chen X, et al. Use of a Physiologically Based Pharmacokinetic Model to Study the Time to Reach Brain Equilibrium : An Experimental Analysis of the Role of Blood-Brain Barrier Permeability , Plasma Protein Binding , and Brain Tissue Binding. 2005; 313: 1254–1262.

Loebstein R, Koren G. Clinical Pharmacology and Therapeutic Drug Monitoring in Neonates and Children. 2016

Lovinger DM. Inhibition of 5-HT3 receptor-mediated ion current by divalent metal cations in NCB-20 neuroblastoma cells. J Neurophysiol 1991; 66: 1329–1337.

Lummis SCR. 5-HT3 receptors. J Biol Chem 2012; 287: 40239–40245.

Mahmood I. Dosing in Children : A Critical Review of the Pharmacokinetic Allometric

Scaling and Modelling Approaches in Paediatric Drug Development and Clinical Settings. 2014: 327–346.

Mason JW, Selness DS, Moon TE, O'Mahony B, Donachie P, Howell J. Pharmacokinetics and repolarization effects of intravenous and transdermal granisetron. 2012

Mcnamara PJ, Alcorn J. Protein Binding Predictions in Infants. 2002; 4

Meszaros P, Hummel I, Klappe K, Draghiciu O, Hoekstra D, Kok JW. The function of the ATP-binding cassette (ABC) transporter ABCB1 is not susceptible to actin disruption. Biochim Biophys Acta - Biomembr 2013; 1828: 340–351.

Metabolism D, Corporation NP, Hanover E, Ag NP. DOSE-DEPENDENT PHARMACOKINETICS OF CYCLOSPORIN A IN RATS : EVENTS IN TISSUES ABSTRACT : 2000; 28: 582–589.

Michelet R. N rs ot on fo al r D U is se tri O bu n tio ly n. 2017

Miller AD, Leslie RA. The area postrema and vomiting. Front Neuroendocrinol 1994; 15: 301–320.

Miller DS, Bauer B, Hart AMS. Modulation of P-glycoprotein at the Blood-Brain Barrier: Opportunities to Improve CNS Pharmacotherapy. Pharmacol Rev 2009; 60: 196–209.

Montaya. modulation-of-3-5-cyclic-amp-homeostasis-in-human-platelets-by-coffee-and-individual-coffee-constituents-div.pdf. 2005

Montoya GA, Bakuradze T, Eirich M, Erk T, Baum M, Habermeyer M, et al. Modulation of $3',5'$-cyclic AMP homeostasis in human platelets by coffee and individual coffee constituents. Br J Nutr 2014; 112: 1427–1437.

Moura CJR de. No Title p . Phys Rev E 2011: 53.

Nakamura H, Ariyoshi N, Okada K, Nakasa H, Nakazawa K, Kitada M. CYP1A1 Is a

Major Enzyme Responsible for the Metabolism of Granisetron in Human Liver Microsomes. Curr Drug Metab 2005; 6: 469–480.

Navari RM. Pharmacological management of chemotherapy-induced nausea and vomiting. Drugs 2009; 69: 515–533.

Navari RM. 5-HT3 receptors as important mediators of nausea and vomiting due to chemotherapy. Biochim Biophys Acta - Biomembr 2015; 1848: 2738–2746.

Nayak S V., Rondé P, Spier AD, Lummis SCR, Nichols RA. Calcium changes induced by presynaptic 5-hydroxytryptamine-3 serotonin receptors on isolated terminals from various regions of the rat brain. Neuroscience 1999; 91: 107–117.

Nestorov I. Whole Body Pharmacokinetic Models. 2003; 42: 883–908.

Nordmark A, Andersson A, Baranczewski P, Wanag E, Ståhle L. Assessment of interaction potential of AZD2066 using in vitro metabolism tools , physiologically based pharmacokinetic modelling and in vivo cocktail data. 2014: 167–178.

Okubo H, Miyake Y, Tanaka K, Sasaki S, Hirota Y. Maternal total caffeine intake, mainly from Japanese and Chinese tea, during pregnancy was associated with risk of preterm birth: The Osaka Maternal and Child Health Study. Nutr Res 2015; 35: 309–316.

Paalzow LK. Torsten Teorell , the Father of Pharmacokinetics Torsten Teorell , the Father of Pharmacokinetics. 2010; 9734

Parkinson A, Mudra DR, Johnson C, Dwyer A, Carroll KM. The effects of gender , age , ethnicity , and liver cirrhosis on cytochrome P 450 enzyme activity in human liver microsomes and inducibility in cultured human hepatocytes. 2004; 199: 193–209.

Parrott N, Hainzl D, Scheubel E, Krimmer S, Boetsch C, Guerini E, et al. Physiologically based absorption modelling to predict the impact of drug properties on pharmacokinetics of

bitopertin. AAPS J 2014; 16: 1077–1084.

Partosch F, Mielke H, Stahlmann R, Gundert-Remy U. Caffeine intake in pregnancy: Relationship between internal intake and effect on birth weight. Food Chem Toxicol 2015; 86: 291–297.

Paul Weathersbee. Caffeine it's direct and indirect effects on reproduction. 1977

Perera V, Elmeliegy MA, Rao G, Forrest A. The link between pharmacodynamics and physiologically based pharmacokinetic models. Clin Pharmacol Ther 2013; 93: 151–152.

Perrine Susan. 基因的改变NIH Public Access. Bone 2005; 23: 1–7.

Pfister M, Eissing T. Physiologically Based Pharmacokinetic Modeling in Pregnancy : A Systematic Review of Published Models. 2018; 104

Plosker GL, Goa KL. Granisetron: A Review of its Pharmacological Properties and Therapeutic Use as an Antiemetic. Drugs 1991; 42: 805–824.

Plowchalk DR, Yeo KR. Prediction of drug clearance in a smoking population : modeling the impact of variable cigarette consumption on the induction of CYP1A2. 2012: 951–960.

Pollack AZ, Buck Louis GM, Sundaram R, Lum KJ. Caffeine consumption and miscarriage: a prospective cohort study. Fertil Steril 2010; 93: 304–306.

Poulin P, Theil F. Prediction of Pharmacokinetics Prior to In Vivo Studies . 1 . Mechanism-Based Prediction of Volume of Distribution. 2002; 91

R. P. Efficacy and safety of granisetron (Kytril) in two special patient populations: children and adults with impaired hepatic function. Semin Oncol 1994; 21: 22–5.

Rhee J, Kim R, Kim Y, Tam M, Lai Y, Keum NN, et al. Maternal caffeine consumption during pregnancy and risk of low birth weight: A dose-response meta-analysis of observational studies [Internet]. PLoS One 2015; 10Available from:

http://dx.doi.org/10.1371/journal.pone.0132334

Von Richter O, Glavinas H, Krajcsi P, Liehner S, Siewert B, Zech K. A novel screening strategy to identify ABCB1 substrates and inhibitors. Naunyn Schmiedebergs Arch Pharmacol 2009; 379: 11–26.

Rieg T, Steigele H, Schnermann J, Richter K, Osswald H, Vallon V. Requirement of intact adenosine A1 receptors for the diuretic and natriuretic action of the methylxanthines theophylline and caffeine. J Pharmacol Exp Ther 2005; 313: 403–409.

Rioux N, Waters NJ. Special Section on Pediatric Drug Disposition and Pharmacokinetics — Minireview Physiologically Based Pharmacokinetic Modeling in Pediatric Oncology Drug Development. 2016: 934–943.

Roche. Granisetron hydrochloride (Kyrtil). Suicide 2013; 3: 1–26.

Rodgers T, Rowland M. Mechanistic Approaches to Volume of Distribution Predictions : Understanding the Processes. 2007; 24: 918–933.

Schlender J, Meyer M, Thelen K, Krauss M, Willmann S, Eissing T, et al. Development of a Whole-Body Physiologically Based Pharmacokinetic Approach to Assess the Pharmacokinetics of Drugs in Elderly Individuals. Clin Pharmacokinet 2016; 55: 1573–1589.

Schmidt AW, Peroutka SJ. Three-dimensional steric molecular modeling of the 5-hydroxytryptamine3 receptor pharmacophore. Mol Pharmacol 1989; 36: 505–511.

Schwen LO, Krauss M, Niederalt C, Gremse F, Kiessling F, Schenk A, et al. Spatio-Temporal Simulation of First Pass Drug Perfusion in the Liver. 2014; 10

Sissung TM, Gardner ER, Piekarz RL, Howden R, Chen X, Woo S, et al. Impact of ABCB1 allelic variants on QTc interval prolongation. Clin Cancer Res 2011; 17: 937–946.

Smith C, Smith M, Cunningham R, Davis S. Recent Advances in Antiemetics. Cancer

Nurs 2019; 00: 1.

De Sousa Mendes M, Hirt D, Urien S, Valade E, Bouazza N, Foissac F, et al. Physiologically-based pharmacokinetic modeling of renally excreted antiretroviral drugs in pregnant women. Br J Clin Pharmacol 2015; 80: 1031–1041.

Spartinou A, Nyktari V, Papaioannou A. Granisetron: a review of pharmacokinetics and clinical experience in chemotherapy induced - nausea and vomiting. Expert Opin Drug Metab Toxicol 2017; 13: 1289–1297.

Suehiro K, Kakutani H, Nakamura K, Morikage N, Yamashita O, Harada T, et al. Immediate Changes to Skin and Subcutaneous Tissue Strains Following Manual Lymph Drainage in Legs with Lymphedema. Ann Vasc Dis 2016; 9: 30–34.

Sugita S, Shen KZ, North RA. 5-hydroxytryptamine is a fast excitatory transmitter at 5-HT3 receptors in rat amygdala. Neuron 1992; 8: 199–203.

Szeto KX, Lukacova V, Woltosz WS, Bolger MB. MembranePlus TM : A Tool to Study In Vitro / In Vivo Transport and Drug-drug Interaction. 2007; 67: 93534.

Tang-Liu D, Williams R, Riegelman S. Disposition of caffeine and its metabolites in man. J Pharmacol Exp Ther 1983; 224: 180–185.

Tapper H, Sundler R. Bafilomycin A1 inhibits lysosomal, phagosomal, and plasma membrane H+-ATPase and induces lysosomal enzyme secretion in macrophages. J Cell Physiol 1995; 163: 137–144.

Taylor P, Thompson CM, Johns DO, Sonawane B, Barton HA, Tardif R, et al. Journal of Toxicology and Environmental Health , Part B : Critical Reviews Database for Physiologically Based Pharmacokinetic (PBPK) Modeling : Physiological Data for Healthy and Health-Impaired Elderly. 2009: 37–41.

Tecott LH, Maricqt4 A V, Juliust D. Nervous system distribution of the serotonin 5-HT3 receptor mRNA (hippocampal formation/amygdala/entorhinal cortex, dorsal raphe nucleus). Proc Nati Acad Sci USA 1993; 90: 1430–1434.

Templeton IE, Jones NS, Musib L. Pediatric Dose Selection and Utility of PBPK in Determining Dose. 2018: 1–9.

Thiel C, Schneckener S, Krauss M, Ghallab A, Hofmann UTE, Kanacher T, et al. A Systematic Evaluation of the Use of Physiologically Based Pharmacokinetic Modeling for Cross-Species Extrapolation. 2014: 1–16.

Tracy TS, Venkataramanan R, Glover DD, Caritis SN. Temporal changes in drug metabolism (CYP1A2, CYP2D6 and CYP3A Activity) during pregnancy. Am J Obstet Gynecol 2005; 192: 633–639.

Tsuji D, Kim Y Il, Nakamichi H, Daimon T, Suwa K, Iwabe Y, et al. Association of ABCB1 polymorphisms with the antiemetic efficacy of granisetron plus dexamethasone in breast cancer patients. Drug Metab Pharmacokinet 2013; 28: 299–304.

Tsuji D, Yokoi M, Suzuki K, Daimon T, Nakao M, Ayuhara H, et al. Influence of ABCB1 and ABCG2 polymorphisms on the antiemetic efficacy in patients with cancer receiving cisplatin-based chemotherapy: A TRIPLE pharmacogenomics study. Pharmacogenomics J 2017; 17: 435–440.

Ufuk A, Somers G, Houston JB, Galetin A. In Vitro Assessment of Uptake and Lysosomal Sequestration of Respiratory Drugs in Alveolar Macrophage Cell Line NR8383. Pharm Res 2015; 32: 3937–3951.

Umemura T, Ueda K, Nishioka K, Hidaka T, Takemoto H, Nakamura S, et al. Effects of Acute Administration of Caffeine on Vascular Function. Am J Cardiol 2006; 98: 1538–1541.

Varma M V, Pang KS, Isoherranen N, Zhao P. Dealing with the complex drug – drug interactions : Towards mechanistic models. 2015; 92: 71–92.

Verscheijden LFM, Koenderink JB, de Wildt SN, Russel FGM. Development of a physiologically-based pharmacokinetic pediatric brain model for prediction of cerebrospinal fluid drug concentrations and the influence of meningitis. PLoS Comput Biol 2019; 15: 1–19.

Weng X, Odouli R, Li D-K. Maternal caffeine consumption during pregnancy and the risk of miscarriage: a prospective cohort study. Am J Obstet Gynecol 2008; 198: 279.e1-279.e8.

Westerhout J, Danhof M, Lange ECMDE. Preclinical Prediction of Human Brain Target Site Concentrations : J Pharm Sci 2011; 100: 3577–3593.

WHO. WHO recommendation on antenatal care for positive pregnancy experience. 2016

Wright DFB, Winter HR, Duffull SB. Understanding the time course of pharmacological effect: A PKPD approach. Br J Clin Pharmacol 2011; 71: 815–823.

Xia B, Heimbach T, Gollen R, Nanavati C, He H. A simplified PBPK modeling approach for prediction of pharmacokinetics of four primarily renally excreted and CYP3A metabolized compounds during pregnancy. AAPS J 2013; 15: 1012–1024.

Yarker YE, Mctavish D, Monteluce P, Hainsworth JD, Sarah T, Cancer C, et al. Granisetron. 1994; 48: 761–762.

Yeo KR, Aarabi M. Modeling and predicting drug pharmacokinetics in patients with renal impairment. 2011: 261–274.

Zhang L, Zhang YD, Zhao P, Huang S. Predicting Drug – Drug Interactions : An FDA Perspective. 2009; 11: 300–306.

Zhang Y, Sriraman SK, Kenny HA, Luther E, Torchilin V, Lengyel E. Reversal of chemoresistance in ovarian cancer by co-delivery of a P-glycoprotein inhibitor and paclitaxel in

a liposomal platform. Mol Cancer Ther 2016; 15: 2282–2293.

Zhao Y, Chen HJ, Caritis S, Venkataramanan R. Development and validation of a sensitive liquid chromatographic-tandem mass spectrometric method for the simultaneous analysis of granisetron and 7-hydroxy granisetron in human plasma and urine samples: Application in a clinical pharmacokinetic study in . Biomed Chromatogr 2016; 30: 149–154.

Zhitomirsky B, Assaraf YG. Lysosomal sequestration of hydrophobic weak base chemotherapeutics triggers lysosomal biogenesis and lysosomedependent cancer multidrug resistance. Oncotarget 2015; 6: 1143–1156.

Zhitomirsky B, Assaraf YG. Lysosomal accumulation of anticancer drugs triggers lysosomal exocytosis. Oncotarget 2017; 8: 45117–45132.

Zhong W, Hutchinson TE, Chebolu S, Darmani NA. Serotonin 5-HT3 receptor-mediated vomiting occurs via the activation of Ca2+/CaMKII-dependent ERK1/2 signaling in the least shrew (Cryptotis parva). PLoS One 2014; 9

Zhou SF. Structure, function and regulation of P-glycoprotein and its clinical relevance in drug disposition. 2008

Zhou Y, Jiang J, Hu P, Wang H. A high-performance liquid chromatography-tandem mass spectrometry method coupled with protein precipitation for determination of granisetron in human plasma and its application to a comparative pharmacokinetic study. Biomed Chromatogr 2014; 28: 1597–1600.

Zoto T, Kilickap S, Yasar U, Celik I, Bozkurt A, Babaoglu MO. Improved Anti-Emetic Efficacy of 5-HT3 Receptor Antagonists in Cancer Patients with Genetic Polymorphisms of ABCB1 (MDR1) Drug Transporter. Basic Clin Pharmacol Toxicol 2015; 116: 354–360.